Table 2
In vitro functional screening of the 12 candidate genes.

Probe set ID	Gene symbol	Gene name	Criteria for selection	*p* value	[^{3}H]PA intake	Fluorescence of Alamar blue	Cellular morphology
Genes relevant to clinical parameters							
75678_at	*MYLK3*	Myosin light chain kinase 3	Correlation with PAP ($r = 0.792$)	0.00262	No change	No change	Spiking
49333_at	*XPR1*	Xenotropic and polytropic retrovirus receptor	Correlation with PAP ($r = 0.765$), GPCR, change in CHF	0.00045	No change	No change	No change
38435_at	*PRDX4*	Peroxiredoxin 4	Correlation with BNP ($r = 0.863$)	0.00024	Increased	Decreased	No change
45314_at	*SMOC2*	SPARC related modular calcium binding 2	Correlation with both PAP and BNP ($r = 0.715$ and 0.758, respectively)	0.00444	No change	No change	No change
Genes encoding orphan GPCRs							
35544_at	*GPR37L1*	G-protein-coupled receptor 37 like 1	Orphan GPCR, downregulated in CVD	>0.005	Decreased	Decreased	Apoptosis
31700_at	*GPR35*	G-protein-coupled receptor 35	Orphan GPCR, upregulated in MI	0.00216	Decreased	Decreased	Hypertrophy
45204_at	*F2RL2*	Coagulation factor II (thrombin) receptor-like 2	GPCR, change in CVD	>0.005	Increased	No change	No change
40299_at	*GPR161*	G-protein-coupled receptor 161	GPCR, expression in heart	>0.005	Decreased	Decreased	No change
Genes encoding interesting enzymes or ion-channels							
38950_at	*MMP23B*	Matrix metallopeptidase 23B	Family of MMP, change in CHF	>0.005	No change	Decreased	No change
35285_at	*NBC1*	Na^+–HCO^{3-} cotransporter 1	Expression in heart	>0.005	No change	Decreased	No change
87788_at	*RHOQ*	Ras homolog gene family, member Q	Expression in DCM, correlation with BNP ($r = 0.711$)	>0.005	No change	No change	No change
78801_at	*STK38*	Serine/threonine kinase 38	Kinase activity, correlation with PAP ($r = 0.736$)	>0.005	No change	No change	No change

PAP, pulmonary artery pressure; GPCR, G-protein-coupled receptor; CHF, congestive heart failure; BNP, brain natriuretic peptide; CVD, cardiovascular disease; MI, myocardial infarction; DCM, dilated cardiomyopathy; PA, phenylalanine. *p* value indicates the significance of the difference between the gene expression level of failing and non-failing myocardium.

gene promoted [^{3}H]phenylalanine incorporation; and the overexpression of six genes lowered the viability of cardiomyocytes, which was evaluated by Alamar blue assay. We also evaluated the phenotype of transfected cardiomyocytes. Unlike control cells, *MYLK3*-adenovirus-transfected cardiomyocytes were spike shaped. The overexpression of *GPR37L1* induced apoptosis of cardiomyocytes. The transfection of *NBC1*-adenoviral vectors modified the beating rate of cardiomyocytes (data not shown). Then, we analyzed each gene that encoded a distinct cardiomyocyte phenotype by developing gene-targeted mouse models.

In vivo analysis using transgenic and knockout mice

To study the *in vivo* role of the selected genes, we developed genetically modified mice: three transgenic (Tg) mice for *Mylk3*, *Gpr37l1*, or *Nbc1* and three knockout (KO) mice for *Gpr37l1*, *Gpr35*, or *Mmp23*. We estimated hemodynamic parameters using Miller catheter and the heart weight (HW)/body weight (BW). As shown in Fig. 2A, we found that the blood pressure of *Gpr37l1*-KO mice was significantly higher than that of *Gpr37l1*-Tg mice by 61.7 mmHg ($p < 0.01$). Further, the blood pressure of *Gpr35*-KO mice was higher than that of wild type (WT) littermate by 37.5 mmHg ($p < 0.01$). Overexpression with or knockout of *Mylk3*, *Mmp23*, or *Nbc1* did not result in a significant change in the systolic blood pressure. The HW/BW of *Mylk3*-Tg mice was lower than that of *Mylk3*-WT mice (Fig. 2B). The HW/BW was higher in *Gpr37l1*-KO mice than in *Gpr37l1*-Tg mice. The HW/BW in mice with *Nbc1*, *Gpr35*, or *Mmp23* manipulations did not show any difference. These data showed that modification of *Gpr37l1*, *Gpr35*, or *Mylk3* can produce a distinct cardiovascular phenotype *in vivo*.

Discussion

The present study identified heart failure-related genes using a novel strategy that was different from the conventional microarray analysis approach. Firstly, we constructed global gene expression profiles to analyze the gene expression in 12 human samples of failing myocardium and two samples of non-failing myocardium. Secondly, we prepared datasets of heart failure-related genes associated with the severity of heart failure; this approach is unique to our study and has not been published before. Thirdly, we selected four genes from these datasets by microarray analysis and a literature-based search. We also included four orphan GPCR genes and four other genes with high expression in the heart as possible drug targets for heart failure treatment. Fourthly, we screened the *in vitro* functions of these 12 genes by achieving adenovirus-mediated overexpression of these genes in rat cardiomyocytes. Finally, we generated gene-targeted mouse models of the five selected genes and screened the *in vivo* functions of these genes. Our novel strategy using a microarray analysis revealed three potential targets, namely, *MYLK3*, *GPR37L1*, and *GPR35* for diagnosing and managing heart failure.

End-stage heart failure caused by a variety of cardiovascular diseases including hypertension, cardiomyopathy, and ischemic heart disease features a common phenotype of reduced cardiac function and dilated cardiac chamber. This result strongly suggested the existence of common genes during the development of heart failure, including the genes encoding natriuretic peptides. To identify novel diagnostic or therapeutic targets for heart failure, such as natriuretic peptides, several microarray analyses of genes expressed in failing myocardium have been performed in the last decade by comparing the gene expression levels between different pairs of samples, such as non-failing versus failing hearts [4–6], failing hearts before versus after placement of left-ventricular assisting device [7,8], hypertrophic versus failing hearts [9], ischemic versus non-ischemic hearts [10]. However, the severity of heart failure is not fixed, but varies from mild to severe heart failure in these studies. To identify the therapeutic targets for heart failure effectively, we believe that it is important to consider the severity of heart failure with microarray data analysis. In this study, we prepared new datasets of heart failure-associated genes that were selected from gene expression profiles of 12 human failing myocardial samples using clinical parameters. A number of genes were associated with PAP, which is an index for the severity of heart failure, whereas only two genes correlated with EF, which is an index for cardiac contractility. This result implies that the stress caused to the heart, and not the ability of cardiac contraction, regulates gene expression in heart failure. We also selected heart failure-related genes whose expression correlated to

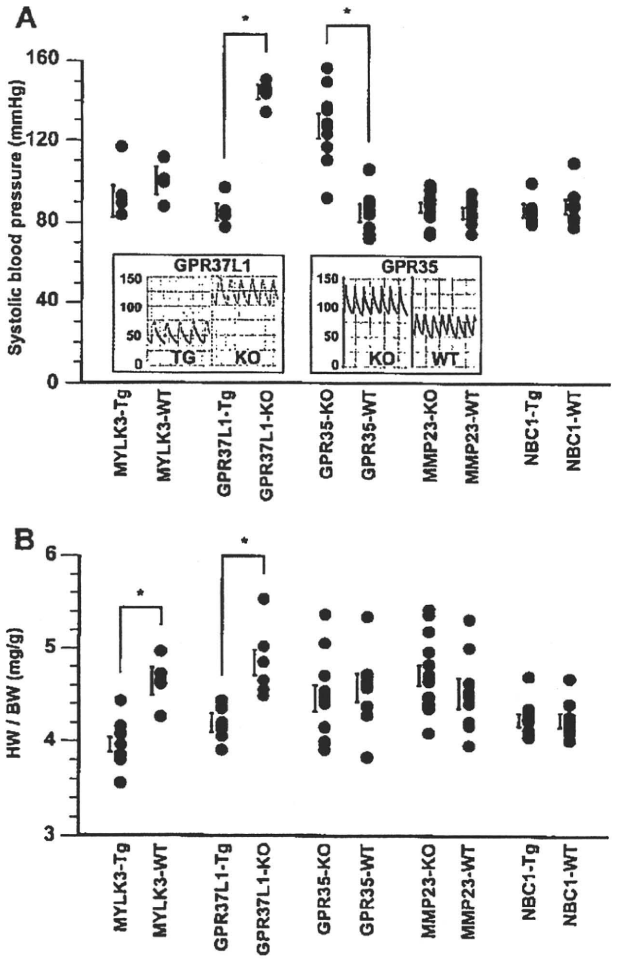

Fig. 2. *In vivo* functional analysis using gene-targeting mice of the *Mylk3*, *Gpr37l1*, *Gpr35*, *Mmp23*, and *Nbc1* genes. Blood pressure and heart weight (HW)/body weight (BW) of transgenic (Tg), knockout (KO) and their wild type (WT) littermate mice of each gene were investigated. Values are means ± SEM. $^*p < 0.01$. (A) Systolic blood pressure measured using Millar catheter inserted via right carotid artery. The monitoring chart shows representative data of *Gpr37l1*- and *Gpr35*-manipulated mice. (B) HW/BW ratio of each gene-targeting mouse.

the BNP mRNA level, which is the best known indicator of heart failure. The approach used in our study can help in efficient identification of the diagnostic or therapeutic targets for heart failure rather than only comparing two types of samples such as failing versus non-failing myocardium. Among the genes from these new datasets, we focused on the genes exhibiting high expression in heart tissues and finally selected four genes for performing the screening of functional analysis *in vitro*. The expression level of *MYLK3* gene was highly correlated to PAP, and this gene was detected only in the heart tissue. Recently, we reported that *MYLK3* plays a crucial role in sarcomere assembly via phosphorylation of myosin regulatory light chain 2V (MLC2v) [13]. We also showed that the knockdown of *MYLK3* by using a morpholino oligo caused immature sarcomere formation leading to ventricular dilation in zebrafish. These results indicate that *MYLK3* is strongly associated with the pathophysiology of heart failure. Chan et al. also reported that MYLK3 phosphorylates MLC2v and regulates sarcomere organization [15]. These reports affirm the reliability of our original strategy that involves the microarray analysis of failing myocardium. Among these genes, most genes including *XPR1*, *PRDX4*, and *SMOC2* have not been reported to link with cardiovascular phenotypes and were not included in many gene expression profiles published previously.

Next, we performed *in vivo* functional analysis of five selected genes, and we found that gene-targeted mouse models of *Mylk3*, *Gpr37l1*, or *Gpr35* showed the cardiovascular phenotype. As described above, *Mylk3* plays a crucial role in failing heart. In this study, we identified two GPCRs, namely, *Gpr37l1* and *Gpr35*, whose modification affects systolic blood pressure or HW/BW. To our knowledge, this is the first report about the role of these genes in cardiovascular system.

GPCRs constitute one of the largest protein families, but many GPCRs remain to be orphaned. GPR35 is now known to have some ligands such as kynurenic acid (KYNA) [16], zaprinast [17], and 5-nitro-2-(3-phenylpropylamino) benzoic acid [18]. These agonists mobilize intracellular calcium concentration. Therefore, lowering systolic blood pressure in *Gpr35*-KO mice can be induced by modulating calcium release from calcium-storing organelles. Among the three agonists, only KYNA is produced endogenously as a metabolite of tryptophan. Although GPR35 gene expression is supposed to be specific to immune cells and gastrointestinal tract, we found that GPR35 gene expression increased in failing myocardium. In an inflammatory state, interferon γ induces idolemine 2,3-dioxygenase, a rate-limiting enzyme involved in tryptophan degradation, resulting in a substantial increase in KYNA. Inflammation is thought to be involved in the pathogenesis of dilated cardiomyopathy as well as myocardial infarction. Hence there is a possibility that a KYNA-GPR35 signaling plays a role in the pathogenesis of cardiovascular diseases.

Unlike GPR35, GPR37L1 is still orphaned. However, we found that *Gpr37l1*-KO mice showed significant high blood pressure and high HW/BW as compared to Tg mice, which implies the existence of cardiovascular-related function of *Gpr37l1*. Identification of the ligand and the function of this orphan receptor are awaited.

Although no significant phenotype was observed in *Mmp23* and *Nbc1*-Tg mice, we have been investigating their cardiac function in pathological condition such as myocardial infarction or hypertension and determined their detrimental effect on heart failure (data not shown).

In the present study, we determined 12 novel heart failure-related genes by integrating an original method with parameters that indicated disease severity. Further, we assessed these possible targets of drug discovery. *MYLK3*, *GPR37L1*, and *GPR35* were the newly identified targets that play an interesting role in the cardiovascular system.

Acknowledgments

This study was supported by Grant-in-Aid for Scientific Research (C) in Japan Society for the Promotion of Science; a grant from Human Genome Tissue Engineering and Food Biotechnology in Health and Labor Science Research from the Ministry of Health, Labor, and Welfare, Japan; and a grant from Japan Cardiovascular Research Foundation.

Appendix A. Supplementary data

Supplementary data associated with this article can be found, in the online version, at doi:10.1016/j.bbrc.2010.01.076.

References

[1] Effect of enalapril on survival in patients with reduced left ventricular ejection fractions and congestive heart failure. The SOLVD Investigators, N. Engl. J. Med. 325 (1991) 293–302.
[2] Effect of metoprolol CR/XL in chronic heart failure: metoprolol CR/XL randomised intervention trial in congestive heart failure (MERIT-HF). Lancet 353 (1999) 2001–2007.

[3] M. Packer, M.R. Bristow, J.N. Cohn, W.S. Colucci, M.B. Fowler, E.M. Gilbert, N.H. Shusterman, The effect of carvedilol on morbidity and mortality in patients with chronic heart failure. U.S. Carvedilol Heart Failure Study Group, N. Engl. J. Med. 334 (1996) 1349–1355.
[4] J. Yang, C.S. Moravec, M.A. Sussman, N.R. DiPaola, D. Fu, L. Hawthorn, C.A. Mitchell, J.B. Young, G.S. Francis, P.M. McCarthy, M. Bond, Decreased SLIM1 expression and increased gelsolin expression in failing human hearts measured by high-density oligonucleotide arrays, Circulation 102 (2000) 3046–3052.
[5] J.D. Barrans, P.D. Allen, D. Stamatiou, V.J. Dzau, C.C. Liew, Global gene expression profiling of end-stage dilated cardiomyopathy using a human cardiovascular-based cDNA microarray, Am. J. Pathol. 160 (2002) 2035–2043.
[6] F.L. Tan, C.S. Moravec, J. Li, C. Apperson-Hansen, P.M. McCarthy, J.B. Young, M. Bond, The gene expression fingerprint of human heart failure, Proc. Natl. Acad. Sci. USA 99 (2002) 11387–11392.
[7] B.C. Blaxall, B.M. Tschannen-Moran, C.A. Milano, W.J. Koch, Differential gene expression and genomic patient stratification following left ventricular assist device support, J. Am. Coll. Cardiol. 41 (2003) 1096–1106.
[8] J.L. Hall, E.J. Birks, S. Grindle, M.E. Cullen, P.J. Barton, J.E. Rider, S. Lee, S. Harwalker, A. Mariash, N. Adhikari, N.J. Charles, L.E. Felkin, S. Polster, R.S. George, L.W. Miller, M.H. Yacoub, Molecular signature of recovery following combination left ventricular assist device (LVAD) support and pharmacologic therapy, Eur. Heart J. 28 (2007) 613–627.
[9] J. Rysa, H. Leskinen, M. Ilves, H. Ruskoaho, Distinct upregulation of extracellular matrix genes in transition from hypertrophy to hypertensive heart failure, Hypertension 45 (2005) 927–933.
[10] M.M. Kittleson, S.Q. Ye, R.A. Irizarry, K.M. Minhas, G. Edness, J.V. Conte, G. Parmigiani, L.W. Miller, Y. Chen, J.L. Hall, J.G. Garcia, J.M. Hare, Identification of a gene expression profile that differentiates between ischemic and nonischemic cardiomyopathy, Circulation 110 (2004) 3444–3451.
[11] A.S. Barth, R. Kuner, A. Buness, M. Ruschhaupt, S. Merk, L. Zwermann, S. Kaab, E. Kreuzer, G. Steinbeck, U. Mansmann, A. Poustka, M. Nabauer, H. Sultmann, Identification of a common gene expression signature in dilated cardiomyopathy across independent microarray studies, J. Am. Coll. Cardiol. 48 (2006) 1610–1617.
[12] M. Asakura, M. Kitakaze, Global gene expression profiling in the failing myocardium, Circ. J. 73 (2009) 1568–1576.
[13] O. Seguchi, S. Takashima, S. Yamazaki, M. Asakura, Y. Asano, Y. Shintani, M. Wakeno, T. Minamino, H. Kondo, H. Furukawa, K. Nakamaru, A. Naito, T. Takahashi, T. Ohtsuka, K. Kawakami, T. Isomura, S. Kitamura, H. Tomoike, N. Mochizuki, M. Kitakaze, A cardiac myosin light chain kinase regulates sarcomere assembly in the vertebrate heart, J. Clin. Invest. 117 (2007) 2812–2824.
[14] M. Asakura, M. Kitakaze, S. Takashima, Y. Liao, F. Ishikura, T. Yoshinaka, H. Ohmoto, K. Node, K. Yoshino, H. Ishiguro, H. Asanuma, S. Sanada, Y. Matsumura, H. Takeda, S. Beppu, M. Tada, M. Hori, S. Higashiyama, Cardiac hypertrophy is inhibited by antagonism of ADAM12 processing of HB-EGF: metalloproteinase inhibitors as a new therapy, Nat. Med. 8 (2002) 35–40.
[15] J.Y. Chan, M. Takeda, L.E. Briggs, M.L. Graham, J.T. Lu, N. Horikoshi, E.O. Weinberg, H. Aoki, N. Sato, K.R. Chien, H. Kasahara, Identification of cardiac-specific myosin light chain kinase, Circ. Res. 102 (2008) 571–580.
[16] J. Wang, N. Simonavicius, X. Wu, G. Swaminath, J. Reagan, H. Tian, L. Ling, Kynurenic acid as a ligand for orphan G protein-coupled receptor GPR35, J. Biol. Chem. 281 (2006) 22021–22028.
[17] Y. Taniguchi, H. Tonai-Kachi, K. Shinjo, Zaprinast, a well-known cyclic guanosine monophosphate-specific phosphodiesterase inhibitor, is an agonist for GPR35, FEBS Lett. 580 (2006) 5003–5008.
[18] Y. Taniguchi, H. Tonai-Kachi, K. Shinjo, 5-Nitro-2-(3-phenylpropylamino)-benzoic acid is a GPR35 agonist, Pharmacology 82 (2008) 245–249.

Journal of Molecular and Cellular Cardiology 48 (2010) 1280–1289

Contents lists available at ScienceDirect

Journal of Molecular and Cellular Cardiology

journal homepage: www.elsevier.com/locate/yjmcc

Original article

X-box binding protein 1 regulates brain natriuretic peptide through a novel AP1/CRE-like element in cardiomyocytes

Tamaki Sawada [a], Tetsuo Minamino [a,*], Hai Ying Fu [a], Mitsutoshi Asai [a], Keiji Okuda [a], Tadashi Isomura [b], Satoru Yamazaki [c], Yoshihiro Asano [a], Ken-ichiro Okada [a], Osamu Tsukamoto [d], Shoji Sanada [d], Hiroshi Asanuma [e], Masanori Asakura [d], Seiji Takashima [a], Masafumi Kitakaze [d], Issei Komuro [a]

[a] Department of Cardiovascular Medicine, Osaka University Graduate School of Medicine, Suita, Osaka 565-0871, Japan
[b] Department of Cardiovascular Surgery, Hayama Heart Center, 1898 Shimoyamaguchi, Hayama, Kanagawa 240-0116, Japan
[c] Department of Cardiovascular Dynamics, National Cardiovascular Center, Suita, Osaka 565-8565, Japan
[d] Department of Cardiovascular Medicine, National Cardiovascular Center, Suita, Osaka 565-8565, Japan
[e] Department of Emergency Room Medicine, Kinki University School of Medicine, Sayama, Osaka 589-8511, Japan

ARTICLE INFO

Article history:
Received 4 October 2009
Received in revised form 2 February 2010
Accepted 3 February 2010
Available online 17 February 2010

Keywords:
Endoplasmic reticulum
Unfolded protein response
XBP1
Brain natriuretic peptide
AP1/CRE-like element
Transcriptional regulation

ABSTRACT

The unfolded protein response (UPR) is triggered to assist protein folding when endoplasmic reticulum (ER) function is impaired. Recent studies demonstrated that ER stress can also induce cell-specific genes. In this study, we examined whether X-box binding protein 1 (XBP1), a major UPR-linked transcriptional factor, regulates the expression of brain natriuretic peptide (BNP) in cardiomyocytes. In samples from failing human hearts, extensive splicing of XBP1 was observed along with increased expression of glucose-regulated protein of 78 kDa (GRP78), a target of spliced XBP1 (sXBP1), suggesting that the UPR was induced in heart failure in humans. Interestingly, quantitative real-time PCR revealed a positive correlation between cardiac expression of GRP78 and BNP, leading us to test the hypothesis that sXBP1 regulates BNP as well as GRP78 in cardiomyocytes. A pharmacological ER stressor caused a dose-dependent increase in the expression of sXBP1 and BNP by cultured cardiomyocytes. Short interfering RNA targeting XBP1 suppressed the induction of BNP expression by a pharmacological ER stressor or norepinephrine, which was rescued by the adenovirus-mediated overexpression of sXBP1. The promoter assay with overexpression of sXBP1 or norepinephrine showed that the proximal AP1/CRE-like element in the promoter region of BNP was critical for transcriptional regulation of BNP by sXBP1. Direct binding of sXBP1 to this element was confirmed by the chromatin immunoprecipitation assay. These findings suggest that ER stress observed in failing hearts regulates cardiac BNP expression through a novel promoter region of the AP1/CRE-like element.

1. Introduction

The endoplasmic reticulum (ER) is an organelle that synthesizes and folds both secretory and membrane proteins [1–3]. Stresses that interfere with ER function lead to the accumulation of unfolded and misfolded proteins, after which the ER transmembrane sensors detect their accumulation and initiate the unfolded protein response (UPR) to maintain ER function [1–3]. Recently, we and others have demonstrated the increased expression of genes targeted by the UPR, such as glucose-regulated protein of 78 kDa (GRP78) and protein disulfide isomerase, in patients with cardiovascular disease, suggesting that activation of the UPR is involved in the pathophysiology of such diseases [1,4,5].

The transcriptional factor X-box binding protein 1 (XBP1) is uniquely regulated by inositol requiring kinase 1α (IRE1α), which is an ER stress sensor conserved in all eukaryotic cells [6]. Interestingly, when IRE1α is activated and senses unfolded proteins in the ER, it promotes an increase of endoribonuclease activity that specifically cleaves the mRNA encoding XBP1 (unspliced XBP1) to form transcriptionally active XBP1 (spliced XBP1) [1–3,6]. Spliced XBP1 (sXBP1) binds to ER stress response elements I and II (ERSE-I; CCAAT (N9)CCACG; ERSE-II; ATTGG(N1)CCACG) and mammalian UPR element (mUPRE; TGACGTGG/A) to regulate a variety of UPR target genes that include ER-resident chaperones and genes involved in ER associated protein degradation and lipid biosynthesis [7,8]. In addition to the induction of UPR-related genes by ER stress, recent studies demonstrated that ER stress also induces unexpected genes in

Abbreviations: BNP, brain natriuretic peptide; cDNA, complementary DNA; ER, endoplasmic reticulum; ERSE-I, -II, ER stress response elements I, II; GAPDH, glyceraldehyde-3-phosphate dehydrogenase; GRP78, glucose-regulated protein of 78 kDa; IRE1α, inositol requiring kinase 1α; mUPRE, mammalian UPR element; NE, norepinephrine; RT-PCR, real-time polymerase chain reaction; siRNA, short interfering RNA; sXBP1, spliced X-box binding protein 1; TU, tunicamycin; uXBP1, unspliced X-box binding protein 1; UPR, unfolded protein response.

* Corresponding author. Department of Cardiovascular Medicine, Osaka University Graduate School of Medicine, 2-2 Yamadaoka, Suita, Osaka 565-0871, Japan. Tel.: +81 6 6879 3635; fax: +81 6 6879 3645.
E-mail address: minamino@cardiology.med.osaka-u.ac.jp (T. Minamino).

0022-2828/$ – see front matter © 2010 Elsevier Ltd. All rights reserved.
doi:10.1016/j.yjmcc.2010.02.004

cell type- and condition-specific manner [9,10]. However, the genes altered by the sXBP1 in cardiomyocytes have not been well clarified. In the present study, we found extensive splicing of XBP1 and positive correlation between cardiac expressions of GRP78 and BNP in human normal and failing heart samples. Then we found that sXBP1 regulates BNP expression via a novel region of the BNP promoter in cultured cardiomyocytes. To our knowledge, this is the first information that links the UPR and the natriuretic peptide system which plays an important role in maintenance of the fluid balance and in cardiovascular growth [11].

2. Materials and methods

2.1. Materials

Tunicamycin (TU) and norepinephrine (NE) were purchased from Sigma Chemical Co. (St. Louis, MO, USA). Antibodies for XBP1, α- and β-actin were obtained from Santa Cruz Biotechnology (Santa Cruz, CA, USA). An antibody for HP1α was obtained from Sigma Chemical Co. HS-142-1 was kindly provided by Kirin-Kyowa Pharmaceutical Co. (Tokyo, Japan).

2.2. Human heart tissue samples

Human heart tissue samples were studied according to the protocol approved by the Institutional Review Boards of Hayama Heart Center and Osaka University. We used heart samples of left ventricle from 4 patients with heart failure who underwent partial left ventriculoplasty at Hayama Heart Center. Messenger RNA of 2 control left ventricle heart samples were obtained commercially from Clontech Labs (Mountain View, CA, USA) and Stratagene (La Jolla, CA, USA). Tissue samples were frozen at −80 °C until use for extraction of RNA.

2.3. Analysis of XBP1 mRNA processing

Evaluation of XBP1 mRNA splicing was performed as described previously [12]. In brief, splicing of XBP1 mRNA by activated IRE1 creates a frame shift [6].Complementary DNA (cDNA) was prepared from human heart samples and rat cardiomyocytes. Using this cDNA as a template, PCR was performed with specific primers for XBP1 that covered the splicing site. (Human: sense primer: 5′-CCTTGTAGTTGAGAACCAGG-3′ and anti-sense primer: 5′-GGGGCTTGGTATATATGTGG-3′, rat: sense primer: 5′-ACGAGAGAAAACTCATGG-3′ and anti-sense primer: 5′-ACAGGGTCCAACTTGTCC-3′). The human PCR amplification products were 416 (spliced) and 442 (unspliced) base pairs (bp) in size, respectively. The rat PCR amplification products were 290 (spliced) and 264 (unspliced) base pairs (bp) in size, respectively. The products were separated on 5% polyacrylamide gel, visualized under UV light and quantified by densitometry (Scion Image software).

2.4. Preparation of neonatal rat cardiomyocytes

Primary cultures of cardiomyocytes were prepared from neonatal rat hearts as described previously [13]. All procedures were done in accordance with the guiding principles of Osaka University School of Medicine, the "Position of the American Heart Association on Research Animal Use", and the "Guide for the Care and Use of Laboratory Animals" published by the US National Institute of Health (NIH Publication No. 85-23, revised 1996).

2.5. Immunoblot analysis

Preparation of cardiomyocytes, electrophoresis, immunoblotting, and detection were all done as described previously [13]. Nuclear and cytosolic fractions were separated by Dignam's method [14]. HP1α and beta-actin were used as controls for the nuclear and cytosolic fractions, respectively.

2.6. Quantitative real-time PCR (RT-PCR)

Human or rat samples were prepared according to the Omniscript Reverse Transcription Handbook (QIAGEN Inc.). The primers and probes used for quantification of sXBP1, BNP, GRP78, and GAPDH were all designed according to the manufacturer's protocol (Applied Biosystems, Foster City, CA. https://www.appliedbiosystems.com/). Quantitative RT-PCR was performed as described previously [13].

2.7. RNA interference

We obtained the short interfering RNAs (siRNAs) from B-Bridge International, Inc. to knock-down rat, but not human, XBP1 mRNA (XBP1-1 siRNA: 5′-GAGAAAGCGCUGCGGAGGA-3′, XBP1-2 siRNA: 5′-CUUCAAAGGUAUUCCAAUA-3′) or rat BNP mRNA (BNP siRNA: 5′-CAAACUUGCCACAGUGUAA-3′), as described previously [13]. Bioinformatic analysis reveals that rat siRNA targeting XBP1 did not knock-down human XBP1. Transfection of the siRNAs was performed as described previously [13].

2.8. Adenovirus transduction

Adenoviral vectors containing the genes for LacZ and spliced human XBP1 were prepared as described previously [13]. Adenovirus carrying LacZ or spliced XBP1 was transfected at 24 h after the isolation of cardiomyocytes, and experiments were performed 48 h after transfection.

2.9. Microarray analysis

For microarray analysis, 3 RNA samples of cardiomyocytes transfected with adenovirus carrying LacZ (80 MOI) or spliced XBP1 (80 MOI) for 48 h were used. Cardiac gene expression was determined using GeneChip Rat Genome 230 2.0 Array (Affymetrix). All expression data were normalized by global scaling and analyzed by GeneSpring software (Agilent Technologies).

2.10. Confocal fluorescence microscopy

Cells were plated at a concentration of 1×10^6 cells/plate and viewed with confocal fluorescence microscopy (Radiance 2100 Laser Scanning System, Bio-Rad, Heimei Hempstead, UK), as described previously [13]. Cell surface area was measured using ImageJ (http://rsb.info.nih.gov/ij/) from 30 randomly selected cells per experiment.

2.11. Assessment of cardiomyocyte viability

The viability of cardiomyocytes was evaluated as described previously [13]. The dose of HS-142-1 used in the present study efficiently blocked BNP receptor [15].

2.12. Plasmid construction

Progressive deletion fragments of the 5′ flanking region of the BNP gene were amplified by PCR with sense primers containing an additional Kpn1 site (hBNP-1780F: 5′-GGTACCCCCTGGCAGTGATTATGAGCTTCA-3′, hBNP-238F; 5′-GGTACCGGGACTTGTCTGTGTCTCCA-3′, hBNP-111F; 5′-GGTACCTGATCTCAGAGGCCCGGAATGT-3′, hBNP-101F; 5′-GGTACCGGCCCGGAATGTGGCTGATAAAT-3′) and an antisense primer containing a Hind III site (hBNP+61R; 5′-AAGCTTGCTGCTGCTGCGATGCGTCCCGGTTTGCTT-3′). After digestion with Kpn1 and Hind III, the fragments were inserted between the Kpn1 and Hind

III sites in the firefly luciferase reporter plasmid pGL3-Basic (Promega). A deletion mutant lacking the AP1/CRE-like element was amplified by PCR with a sense primer (hBNP-103F: 5′-GAGGCCCGGAATGTGGCTGATAAAT-3′) and an anti-sense primer (hBNP-112R: 5′-GGGCCCGGGAATGAGCCCCTCCGCGCCT-3′), and was inserted into the pGL3-Basic plasmid. The plasmid for human sXBP1 was a kind gift from Dr. K. Mori (Kyoto University, Japan).

2.13. Luciferase gene reporter assay

Freshly prepared rat cardiomyocytes (4×10^6 cells) were transiently co-transfected with 10 μg of the indicated reporter construct and 10 μg of control vector (Renilla luciferase plasmid pRL-SV40) with or without 10 μg of the effector plasmid carrying sXBP1 cDNA. Electroporation was done at 280 V/300 μF in 0.2-cm cuvettes. Then the cells were plated into fibronectin-coated six-well culture dishes and incubated for 72 h to allow attachment. For the NE experiment, cardiomyocytes were co-transfected with the indicated reporter construct and control vector and maintained for 48 h. Then, they were treated with NE (1 μmol/L) for 24 h. Subsequently, luciferase activity of cell lysates was measured with a luminometer according to the manufacturer's protocol (Dual-Luciferase Reporter Assay; Promega), and reporter activity was calculated as the relative luciferase activity (firefly luciferase/Renilla luciferase) to correct for variations in transfection efficiency.

2.14. Chromatin immunoprecipitation (ChIP) assay

Rat neonatal cardiomyocytes (5×10^6) were transfected with adenovirus carrying human sXBP1 or LacZ and incubated for 48 h before being cross-linked with 1% formaldehyde. The ChIP assay was performed using a Chromatin Immunoprecipitation Assay Kit (Upstate) according to the manufacturer's protocol. The P1/P2 primers used for detection of rat BNP were 5′-GACAACACCAGCTGCAGGATGGGCTTGACGGCAAGT-3′ (rBNP-2863F) and 5′-CCGACCTCTGTGCATCAATGGTA-3′ (rBNP-2706R), yielding a 157 bp product. The P3/P4 primers used for detection of rat BNP were 5-GGAAACAAGGACCTGTTAGTGT-3′ (rBNP-257F) and 5-GGGTGGGGTTATCTCTGATTT-3′ (rBNP-72R), yielding a 185 bp product.

2.15. Statistical analysis

Data are expressed as the mean ± S.E.M. Unpaired Student *t*-test was used to compare the expression of BNP and GRP78 in human hearts. Spearman rank correlation analysis was used to examine the relationship between cardiac mRNA levels of targeted genes. The results of quantitative RT-PCR, cardiomyocyte viability analysis, and the promoter assay were compared by one-way factorial ANOVA followed by Bonferroni's correction. Microarray data was analyzed using unpaired *t*-test. For all analyses, $P<0.05$ was accepted as statistically significant.

3. Results

3.1. Extensive XBP1 splicing and increased expression of GRP78 and BNP in human failing hearts

To investigate activation of the UPR in failing human hearts, we determined the extent of XBP1 mRNA splicing as an indicator of UPR activation in samples of normal and failing myocardium. The clinical characteristics of patients were listed in the Table 1. The major form of XBP1 in normal human hearts was unspliced, while the major form in failing hearts was spliced (Fig. 1A). Consistent with these findings about XBP1 activation, quantitative RT-PCR revealed that expression of GRP78, a target of sXBP1, was significantly higher in failing hearts ($n=4$) than in normal hearts ($n=2$) (Fig. 1B). These findings suggest that the UPR was activated in failing human hearts. In addition, the BNP mRNA level was significantly higher in failing human hearts ($n=4$) compared with that in normal hearts ($n=2$) (Fig. 1C). Importantly, the quantitative real-time PCR revealed a positive correlation between cardiac expressions of GRP and BNP (Fig. 1D). There was no significant correlation between sXBP1 and GRP78 (Fig. 1E) or BNP (Fig. 1F).

Table 1
Clinical characteristics of patients.

Age	Gender	Diagnosis	BNP (pg/mL)	NYHA class	Echocardiographic findings		
					EF (%)	LVDd (mm)	LVDs (mm)
69	M	DCM	465	III	30	86	73
63	M	DCM	621	III	28	68	58
59	M	ICM	104	III	18	71	58
57	M	ICM	166	III	15	77	68

DCM, dilated cardiomyopathy; ICM, ischemic cardiomyopathy; BNP, brain-type natriuretic peptide; NYHA, New York Heart Association function class; LVEF, left ventricular ejection fraction; LVDd, left ventricular end-diastolic dimension; LVDs, left ventricular end-systolic dimension.

3.2. A pharmacological ER stressor increases BNP expression via an XBP1-dependent pathway in rat neonatal cardiomyocytes

Then, we investigated whether ER stress could induce BNP expression via an XBP1 dependent pathway. PCR analysis showed that treatment of cardiomyocytes with tunicamycin (TU), a pharmacological ER stressor, increased the level of mRNA for spliced XBP1 (Fig. 2A). TU increased the protein levels of nuclear, but not cytosolic, XBP1 protein (Fig. 2A) and mRNA levels of BNP (Fig. 2B) in rat cardiomyocytes. When we transfected a different dose of siRNA targeting XBP1 (siRNA-XBP1-1), siRNA targeting XBP1 dose-dependently reduced protein levels of nuclear XBP1 and mRNA levels of BNP by tunicamycin (Fig. 2C). When we transfected 2 different siRNAs targeting XBP1, either of the siRNAs targeting XBP1 efficiently reduced XBP1 protein levels (Fig. 2D). We also found that increased expression of BNP in response to pharmacological ER stress was significantly attenuated by 2 different siRNAs targeting XBP1 (Fig. 2E). These findings suggested that pharmacological ER stress induces BNP expression via an XBP1-dependent pathway in cultured rat cardiomyocytes.

3.3. Adenovirus-mediated overexpression of spliced XBP1 increases BNP expression in cultured rat cardiomyocytes

Next, we investigated the influence of sXBP1 on BNP expression by cultured rat cardiomyocytes. Immunohistological analysis revealed the nuclear localization of XBP1 in rat cardiomyocytes infected with adenovirus carrying sXBP1, but not LacZ (Fig. 3A). The transfection of adenovirus carrying sXBP1 or LacZ did not change the cardiomyocyte size (Fig. 3B). An increase of nuclear XBP1 protein levels by the overexpression of sXBP1 was also confirmed by immunoblot analysis (Fig. 3C). Adenovirus-mediated overexpression of sXBP1 increased mRNA levels of GRP78 (Fig. 3D) and BNP (Fig. 3E) in a dose-dependent manner.

Since the stimuli that enhance BNP expression often activate hypertrophic program, we checked the expression levels of representative hypertrophic genes when cardiomyocytes were transfected with adenovirus carrying LacZ ($n=3$) or sXBP1 ($n=3$): BNP (0.47 ± 0.07 versus 1.47 ± 0.04, $P=0.0002$), GRP78 (0.83 ± 0.12 versus 1.81 ± 0.25, $P=0.02$), β-myosin heavy chain (MHC) (0.93 ± 0.05 versus 1.05 ± 0.04, $P=0.15$), atrial natriuretic peptide (ANP) (0.86 ± 0.08 versus 1.10 ± 0.04, $P=0.06$), α-actin (0.35 ± 0.13 versus 1.46 ± 0.03, $P=0.001$), α-MHC (1.00 ± 0.00 versus 0.73 ± 0.14, $P=0.12$) and sarcoendoplasmic reticulum Ca ATPase (SERCA) (0.96 ± 0.04 versus 0.97 ± 0.19, $P=0.95$). These findings suggest that hypertrophic genes

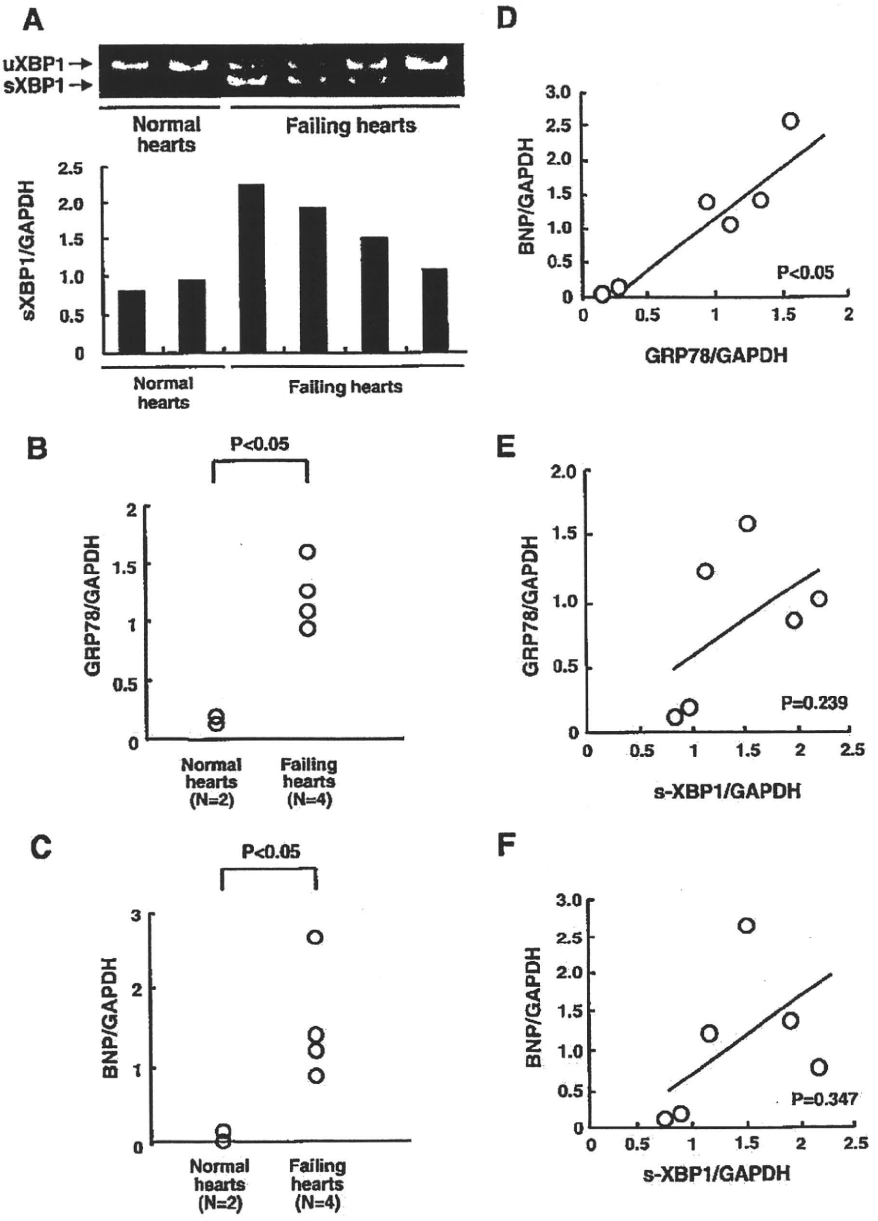

Fig. 1. UPR signaling in human hearts. (A) (Upper panel) Splicing of XBP1 mRNA in myocardial tissue from normal ($n=2$) and failing ($n=4$) human hearts. (Lower panel) Quantitative analysis of sXBP1 in normal and failing human hearts. uXBP1 and sXBP1 indicate unspliced and spliced XBP1, respectively. (B, C) Quantitative analysis of GRP78 (B) and BNP (C) mRNA in normal and failing human hearts. (D) Relationship between the cardiac expression of GRP78 and BNP in normal and failing human hearts. (E, F) Relationship between the cardiac expression of sXBP1 and GRP78 (E) or BNP (F) in normal and failing human hearts. All results of quantitative RT-PCR were normalized for GAPDH expression.

except α-actin did not significantly alter by the overexpression of sXBP1. Furthermore, overexpression of sXBP1 did not alter cardiomyocyte viability, suggesting that sXBP1 did not induce BNP secondary to cellular damage (data not shown). Importantly, we found that overexpression of sXBP1, but not LacZ, could rescue the tunicamycin-mediated enhancement of BNP that was blocked by siRNA for XBP1 (Fig. 3F). We could not detect the binding of XBP1 to the proximal AP1/CRE-like element in the BNP promoter in response to a pharmacological stressor (data not shown).

3.4. Spliced XBP1 binds to an AP1/CRE-like element in the BNP promoter region and increases its promoter activity

To investigate whether or not sXBP1 activated the transcription of BNP, we performed a number of luciferase reporter assays, in which cultured cardiomyocytes were co-transfected with a series of reporter plasmids containing fragments of the BNP 5′-flanking region (from −1780 to −101) and the pGL3 vector with or without sXBP1. Under baseline conditions, transfection of longer reporter plasmids containing the promoter region (−238 to −111) increased luciferase activity compared with transfection of the reporter plasmid lacking the promoter region (−238 to −111) or the empty pGL3-Basic plasmid (Fig. 4A left). These findings suggested that the proximal region (−238 to −111) was essential for BNP promoter activity under baseline conditions. After transfection of the pGL3-Basic vector containing spliced XBP1 (inducible conditions), co-transfection of the reporter gene containing the region (−111 to −101) increased luciferase activity by 3- to 4-fold compared with the control (empty pGL3-Basic vector) or the reporter gene lacking this region (Fig. 4A right). The bioinformatic analysis revealed that the BNP promoter

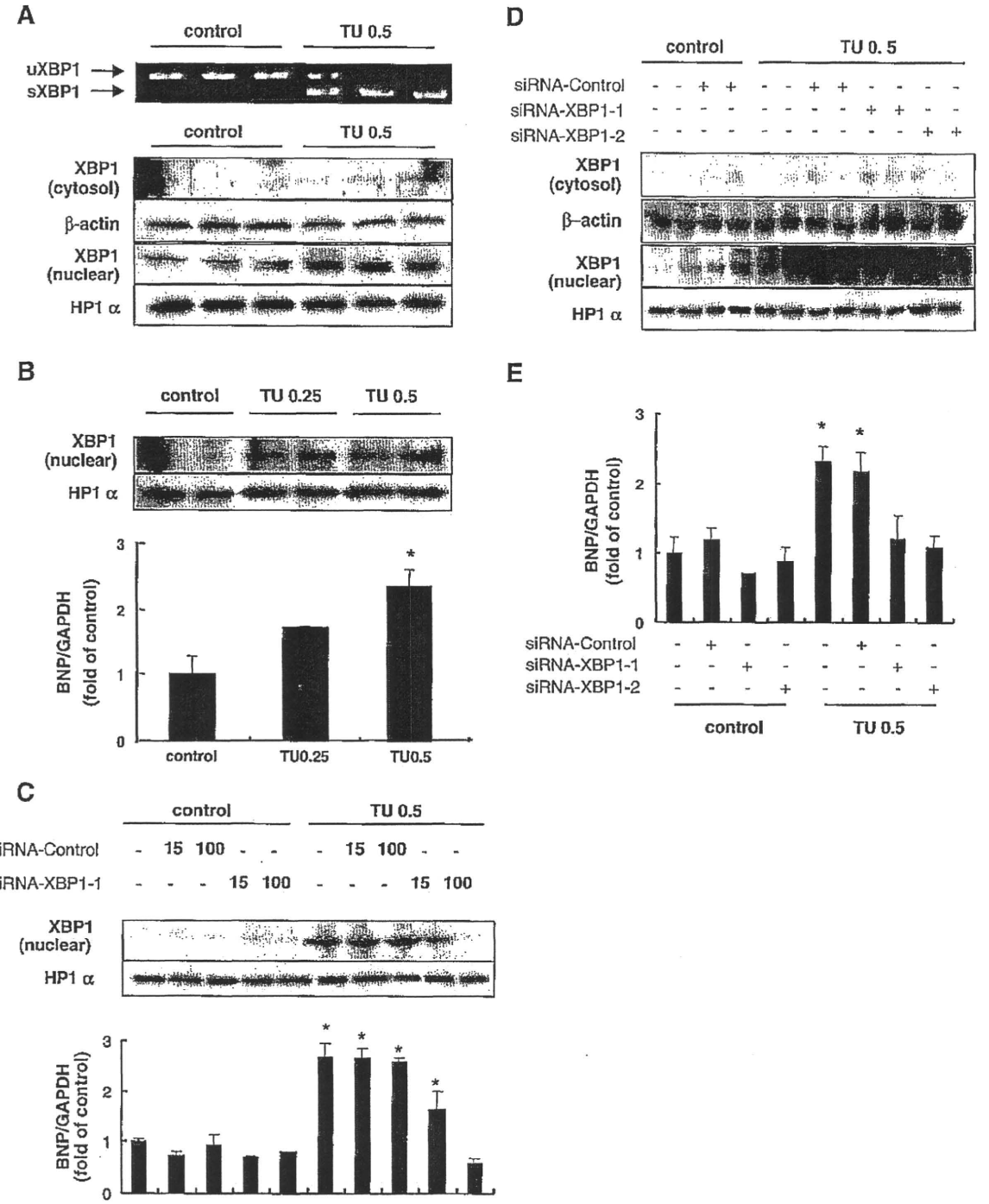

Fig. 2. A pharmacological ER stressor increases BNP expression via an XBP1-dependent pathway in rat neonatal cardiomyocytes. (A) Effects of TU on splicing of XBP1 in cultured cardiomyocytes. Neonatal rat cardiomyocytes were maintained for 24 h and then treated with TU (0.5 μg/mL) for the next 24 h. Evaluation of XBP1 splicing was performed by quantitative RT-PCR (upper panel) and immunoblot analysis (lower panel). (B) Dose-dependent effects of TU (0.25 or 0.5 μg/mL) on protein levels of XBP1 in the nuclear fraction (upper panel) and mRNA levels of BNP (lower panels) in cultured cardiomyocytes. HP1α was used as the internal control for protein levels in nuclear fraction. Results were expressed as the mean ± SEM. *$P<0.05$ versus control. (C) Dose–response effects of siRNA for XBP1 on BNP expression. Neonatal rat cardiomyocytes were maintained for 6 h and then were treated with different dose of control and XBP1 siRNA (15 μmol/L and 100 μmol/L) for 18 h. Subsequently, cardiomyocytes were treated with TU (0.5 μg/mL) for 24 h. (D, E) Effects of 2 different siRNAs targeting XBP1 on the protein level of XBP1 (D) and mRNA level of BNP (E) in cardiomyocytes treated with TU. Experiments were repeated twice independently ($n=2$–3 per experiment). Results are expressed as the mean ± SEM. *$P<0.05$ versus control.

region (−111 to −101) corresponded to an AP1/CRE-like element, which is well conserved among mammals (Fig. 4B). These findings suggested that the AP1/CRE-like element is essential for BNP promoter activity under inducible conditions.

Next, we transfected reporter plasmids containing the BNP promoter region (−1780 to +63) with and without the AP1/CRE-like element (−111 to −101). Deletion of the AP1/CRE-like element resulted in a significant decrease of luciferase activity under inducible

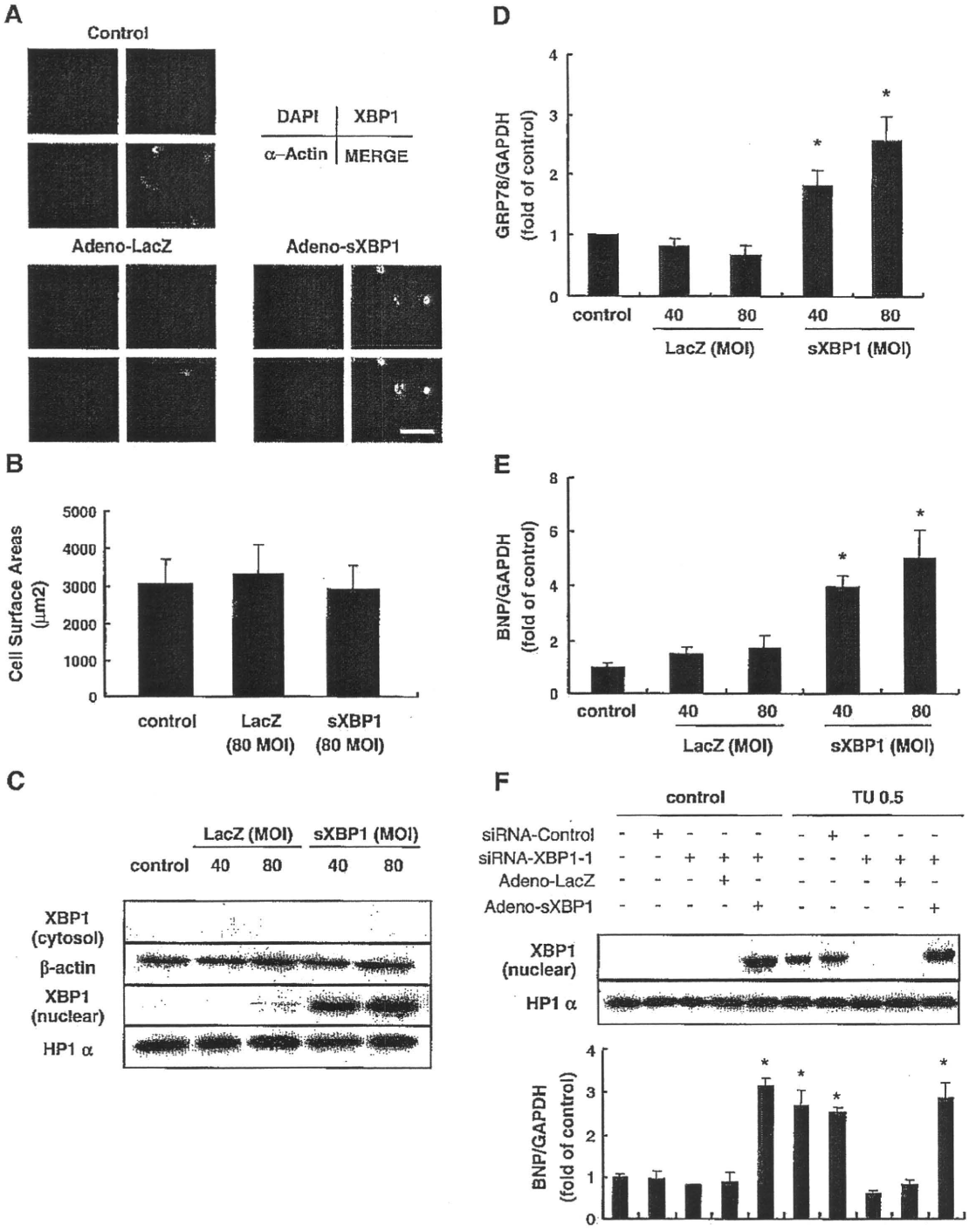

Fig. 3. Adenovirus-mediated overexpression of spliced XBP1 increases BNP expression in neonatal rat cardiomyocytes. (A) Representative immunohistochemistry of XBP1 expression in cultured rat cardiomyocytes. Confocal fluorescence microscopy shows XBP1, α-actin, and DAPI by green, red and blue staining, respectively. Bar indicates 20 μm. (B) Effects of adenovirus-mediated overexpression of LacZ or spliced XBP1 on cardiomyocyte size. (C) Immunoblot analysis of XBP1 in the nuclear and cytosolic fractions. HP1α and β-actin were used as the internal controls for the nuclear and cytosolic fractions, respectively. XBP1 in cytosolic fractions was not observed due to the rapid degradation by proteasome. Effects of overexpression of spliced XBP1 on GRP78 (D) and BNP (E) mRNA levels in cultured cardiomyocytes. MOI indicates multiplicity of infection. (F) Effects of overexpression of XBP1 on mRNA level of BNP that is blocked by siRNA for XBP1. Cardiomyocytes were treated with siRNA targeting XBP1 for 24 h and were treated with tunicamycin (0.5 μg/mL) for the next 24 h. Thereafter, they were incubated with an adenoviral vector carrying LacZ (80 MOI) or spliced XBP1 (80 MOI) for 48 h. Experiments were repeated twice independently ($n=2$–3 per experiment). Results were expressed as the mean ± SEM. *$P<0.05$ versus control.

conditions by overexpression of sXBP1 (Fig. 4C), but not baseline ones.

We also examined the role of XBP1 in BNP expression in response to NE. We found that the NE (1 μmol/L) for 24 h increased protein levels of XBP1 in the nuclear fractions and BNP expression in cultured cardiomyocytes, which was significantly attenuated by siRNA targeting XBP1. The quantitative real-time analysis revealed that the siRNA targeting sXBP1 did not block the enhancement of ANP by NE

(Control: 1.00 ± 0.16; NE: 1.61 ± 0.19; NE + siRNA XBP1: 1.67 ± 0.31; $n=3$ in each group), suggesting that XBP1 is not involved in hypertrophic program in response to NE. These findings suggest that XBP1 is involved in BNP expression in response to NE as well as a pharmacological ER stressor. Deletion of the proximal AP1/CRE-like element resulted in a significant decrease of luciferase activity in response to NE (Fig. 4D).

Finally, we performed the ChIP assay to determine whether sXBP1 binds to the AP1/CRE-like element of the endogenous BNP promoter in vivo. Chromatin from cardiomyocytes transfected with adenovirus carrying LacZ or sXBP1 was immunoprecipitated with an antibody directed against XBP1. PCR products were obtained by using primers that covered the AP1/CRE-like element (P3/P4), but not with primers covering the −2863 to −2706 region (P1/P2) (Fig. 4E).

3.5. Induction of BNP by pharmacological ER stress does not affect the viability of cultured cardiomyocytes

We investigated the effect of the induction of BNP by pharmacological ER stress on cell viability. The siRNA targeting BNP reduced the BNP mRNA level by 93% ($n=4$). There was no difference of cell viability when cardiomyocytes were treated with the siRNA targeting BNP (Fig. 5A) or a BNP receptor antagonist (HS-142-1) followed by a pharmacological ER stressor (Fig. 5B). These findings suggested that the induction of BNP by ER stress did not directly prevent cardiac cell death by ER stress.

4. Discussion

4.1. The UPR in heart failure

The ER is an organelle with a role in protein folding, calcium homeostasis, and lipid biosynthesis. Failing hearts show oxidative stress, hypoxia, and enhanced protein synthesis, any of which could potentially lead to ER dysfunction [1–3]. Indeed, we and others have found extensive splicing of XBP1 and increased expression of GRP78 in failing human hearts, suggesting that the UPR is activated in diseased hearts [6,7,16]. Consistent with previous reports, we also found an increase of BNP mRNA levels in myocardial samples from failing human hearts, which is widely used as a marker of heart failure [11,17]. Although the UPR triggers signaling that induces genes to maintain ER function, recent studies have shown that the UPR is also linked to other physiological systems [9,10]. Interestingly, we found a positive correlation between cardiac expression of GRP78 and BNP in human samples. These findings led us to hypothesize that BNP as well as GRP78 are commonly regulated by an UPR-dependent mechanism, although BNP has not previously been recognized as one of the targets of the UPR. Disappointingly, cardiac expressions of sXBP1 did not correlate with those of GRP78 or BNP probably due to the multiple factors that would modify their cardiac expressions in the clinical settings.

4.2. BNP expression is regulated by XBP1 in cardiomyocytes

To investigate whether BNP expression was regulated by ER stress, we treated cultured cardiomyocytes with a pharmacological ER stressor, tunicamycin, which is an inhibitor of glycosylation. This agent dose-dependently increased the expression of BNP in cultured cardiomyocytes, suggesting that BNP expression is upregulated in response to ER stress. We also confirmed that sXBP1 had a crucial role in the cardiac expression of BNP as well as GRP78 in response to a pharmacological ER stressor by experiments using 2 different siRNAs against XBP1 or an adenovirus vector carrying sXBP1. Since we showed that overexpression of sXBP1 increased BNP expression without affecting cardiomyocyte viability, the elevation of BNP expression did not seem to be due to cellular damage caused by adenoviral transfection.

Many hypertrophic stimuli can enhance BNP expression along with both the activation of hypertrophic program and the increase in cardiomyocytes size [18]. Thus, we performed microarray analysis to check whether overexpression of sXBP1 could alter the representative hypertrophic gene expressions. We found that these genes except α-actin did not significantly alter by the overexpression of sXBP1. Interestingly, bioinformatic analysis reveals that there exists AP1/CRE-like element in the promoter region of α-actin (−520 to −513). These results would strength the findings that sXBP1 could regulate the expression of some genes through the AP1/CRE-like element. Furthermore, the overexpression of sXBP1 did not change the size of cultured cardiomyocytes and the siRNA for sXBP1 did not block the enhancement of ANP by NE. These findings also suggest that sXBP1 enhances BNP expression without altering hypertrophic program.

In addition to sXBP1, several factors are involved in the transcription of genes targeted by the UPR [1–3]. These UPR-linked transcriptional factors independently, and sometimes cooperatively, regulate the target genes in response to ER stress [1–3]. Since 2 different siRNAs targeting XBP1 almost completely suppressed BNP expression by tunicamycin and overexpression of sXBP1 could rescue the tunicamycin-mediated enhancement of BNP that was blocked by siRNA targeting XBP1, sXBP1 seems to be an essential regulator of BNP transcription in response to ER stress.

4.3. Spliced XBP1 binds to the BNP promoter response element and increases its promoter activity

Spliced XBP1 is known to bind to certain promoter regions, including ERSE-I, ERSE-II, and mUPRE [7,8], but our bioinformatics analysis revealed that the promoter region of BNP does not include any of these regions. Surprisingly, the promoter assay revealed that the AP1/CRE-like element (−111 to −103) of the BNP promoter was essential for its enhanced activity by spliced XBP1. The ChIP assay also demonstrated that spliced XBP1 bound to the AP1/CRE-like element. AP-1/CRE-like element is the site overlapped by AP-1 and CRE binding sequence [19,20]. Although several factors are reported to bind to this element, to our knowledge, this is the first to show that sXBP1 can bind to this region. Bioinformatic analysis revealed that BNP promoter has 3 different AP-1/CRE-like elements (TGATCTCA at −111; TGAGATCA at −385; and TGACATCA at −1472). Importantly, the promoter assay analysis demonstrated that the only proximal AP-1/CRE-like element has the function to enhance BNP expression in response to spliced XBP-1. Lapointe et al. demonstrated that the proximal AP1/CRE-like element (−111 to −103) is required for BNP expression in response to mitogen activated protein kinase (MAPK) kinase 6 or p38 MAPK [21]. Consistently, another study also demonstrated that only one specific element can play an important role in gene regulation although several of the same elements exist in the promoter region [22].

Although we performed ChIP assay using a pharmacological ER stressor, we could not detect the binding of XBP1 to the proximal AP1/CRE-like element in the BNP promoter (data not shown). One possible explanation for this failure would be due to the difference in sXBP1 levels in experiments using XBP1 overexpression and pharmacological treatment. Furthermore, we tried to use 2 different antibodies against XBP1 for the ChIP assay, but we could detect the binding only when we used the antibody presented in the manuscript. Thus, the technical limitation would be the possible explanation for the failure to detect the binding using a pharmacological ER stressor.

Recent studies demonstrated that NE can induce ER stress in PC12 cells [23,24]. The present study revealed that NE increased protein levels of sXBP1 and that BNP expression in response to NE was blocked by siRNA against XBP1. Since adrenergic systems are activated in patients with heart failure, increased levels of NE might regulate BNP via ER stress related pathways. Since NE can activate both MAPK- and XBP1-dependnt pathways, further investigation will be required for the interaction between sXBP1 and MAPK in the BNP expression through the proximal Ap1/CRE-like element [20,21].

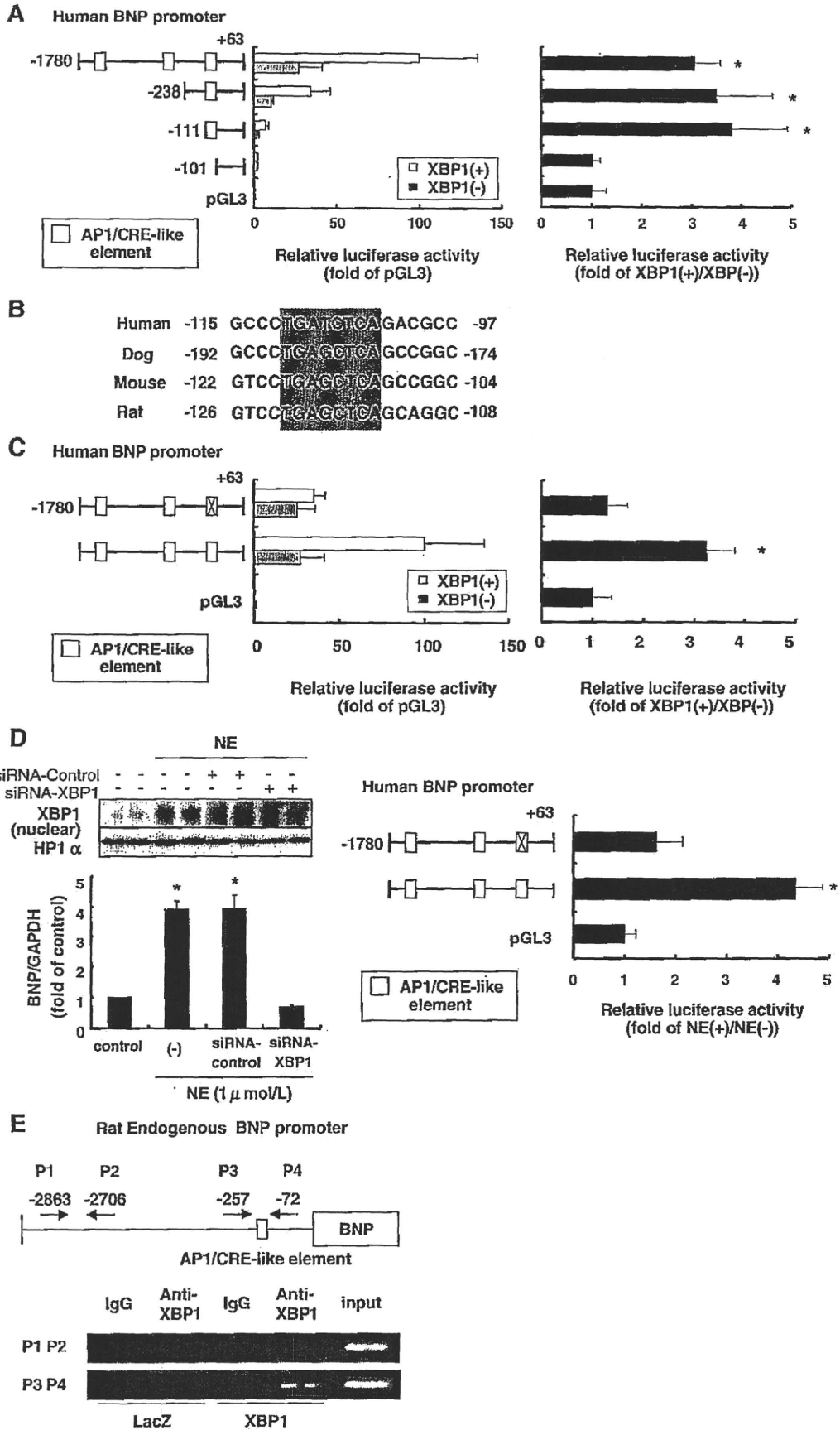
A
Human BNP promoter
+63
-1780
-238
-111
-101
pGL3
AP1/CRE-like element
XBP1(+)
XBP1(-)
0 50 100 150
Relative luciferase activity (fold of pGL3)
0 1 2 3 4 5
Relative luciferase activity (fold of XBP1(+)/XBP(-))
B
Human -115 GCCCTGATCTCAGACGCC -97
Dog -192 GCCCTGAGCTCAGCCGGC -174
Mouse -122 GTCCTGAGCTCAGCCGGC -104
Rat -126 GTCCTGAGCTCAGCAGGC -108
C
Human BNP promoter
+63
-1780
pGL3
AP1/CRE-like element
XBP1(+)
XBP1(-)
0 50 100 150
Relative luciferase activity (fold of pGL3)
0 1 2 3 4 5
Relative luciferase activity (fold of XBP1(+)/XBP(-))
D
NE
siRNA-Control - - - - + + - -
siRNA-XBP1 - - - - - - + +
XBP1 (nuclear)
HP1 α
BNP/GAPDH (fold of control)
0 1 2 3 4 5
control
(-)
siRNA-control
siRNA-XBP1
NE (1 μ mol/L)
Human BNP promoter
+63
-1780
pGL3
AP1/CRE-like element
0 1 2 3 4 5
Relative luciferase activity (fold of NE(+)/NE(-))
E
Rat Endogenous BNP promoter
P1 P2 P3 P4
-2863 -2706 -257 -72
BNP
AP1/CRE-like element
IgG Anti-XBP1 IgG Anti-XBP1 input
P1 P2
P3 P4
LacZ
XBP1

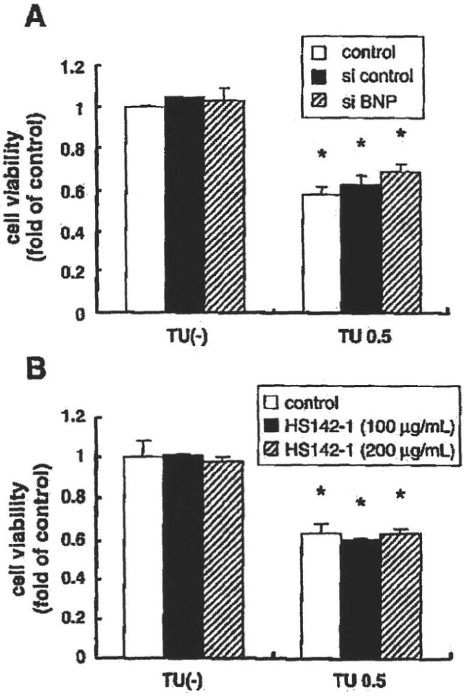

Fig. 5. Induction of BNP by pharmacological ER stress does not affect the viability of cultured cardiomyocytes. Effect of siRNA targeting BNP or HS-142-1, a BNP receptor blocker, on cardiomyocyte death after exposure to pharmacological ER stress with TU. (A) Neonatal rat cardiomyocytes were maintained for 6 h and then treated with BNP siRNA for 18 h. Subsequently, cardiomyocytes were treated with TU (0.5 μg/mL) for 24 h and cell viability was evaluated. (B) Effect of HS-142-1, a BNP receptor blocker, on cardiomyocyte viability after treatment with TU. Neonatal rat cardiomyocytes were maintained for 24 h and then treated with HS-142-1 (100 or 200 μg/mL) for 6 h. Subsequently, the cells were treated with TU (0.5 μg/mL) for 24 h and their viability was evaluated. Three independent experiments were done to assess cell viability ($n=6$ per experiment). *$P<0.05$ versus no treatment.

4.4. Pathophysiological role of BNP induced by XBP1

Since XBP1 mainly regulates UPR-related genes that potentially reduce cell damage due to ER stress, we checked whether the knockdown of BNP mRNA or blockade of the BNP receptor directly influenced cardiac cell viability in response to a pharmacological ER stressor. Our data showed that BNP in response to ER stress did not directly influence cell viability due to ER stress in cardiomyocytes. However, since BNP has an important role in the maintenance of fluid balance and in cardiovascular growth [11], induced BNP by sXBP1 would indirectly contribute to the improvement in cardiac dysfunction in which UPR is activated.

4.5. Conclusion

In the present study, we showed that sXBP1 regulates BNP expression in cultured cardiomyocytes. Regulation of BNP by XBP1 is another intriguing example of integration of the UPR with a range of physiological systems. Furthermore, since BNP is used for the treatment of heart failure [25], drugs targeting spliced XBP1 or the other factors that bind to the AP1/CRE-like element of BNP promoter region could be promising new therapies for heart failure.

Acknowledgments

We thank Dr. Kazutoshi Mori for the generous gift of sXBP1 cDNA and Ms. Akiko Ogai and Mieko Hayakawa for help with the preparation of mRNAs and cardiomyocytes.

This research was supported by grants-in-aid from the Ministry of Health, Labor, and Welfare—Japan; grants-in-aid from the Ministry of Education, Culture, Sports, Science, and Technology—Japan; grants from the Japan Heart Foundation.

References

[1] Minamino T, Kitakaze M. ER stress in cardiovascular disease. J Mol Cell Cardiol Nov 12 2009 Electronic publication ahead of print.
[2] Kaufman RJ. Orchestrating the unfolded protein response in health and disease. J Clin Invest 2002;110:1389–98.
[3] Ron D, Walter P. Signal integration in the endoplasmic reticulum unfolded protein response. Nat Rev Mol Cell Biol 2007;8:519–29.
[4] Okada K, Minamino T, Tsukamoto Y, Liao Y, Tsukamoto O, Takashima S, et al. Prolonged endoplasmic reticulum stress in hypertrophic and failing heart after aortic constriction: possible contribution of endoplasmic reticulum stress to cardiac myocyte apoptosis. Circulation 2004;110:705–12.
[5] Severino A, Campioni M, Straino S, Salloum FN, Schmidt N, Herbrand U, et al. Identification of protein disulfide isomerase as a cardiomyocyte survival factor in ischemic cardiomyopathy. J Am Coll Cardiol 2007;50:1029–37.
[6] Calfon M, Zeng H, Urano F, Till JH, Hubbard SR, Harding HP, et al. IRE1 couples endoplasmic reticulum load to secretory capacity by processing the XBP-1 mRNA. Nature 2002;415:92–6.
[7] Yamamoto K, Yoshida H, Kokame K, Kaufman RJ, Mori K. Differential contributions of ATF6 and XBP1 to the activation of endoplasmic reticulum stress-responsive cis-acting elements ERSE, UPRE and ERSE-II. J Biochem 2004;136:343–50.
[8] Lee AH, Iwakoshi NN, Glimcher LH. XBP-1 regulates a subset of endoplasmic reticulum resident chaperone genes in the unfolded protein response. Mol Cell Biol 2003;23:7448–59.
[9] Acosta-Alvear D, Zhou Y, Blais A, Tsikitis M, Lents NH, Arias C, et al. XBP1 controls diverse cell type- and condition-specific transcriptional regulatory networks. Mol Cell 2007;27:53–66.
[10] Kaser A, Lee AH, Franke A, Glickman JN, Zeissig S, Tilg H, et al. XBP1 links ER stress to intestinal inflammation and confers genetic risk for human inflammatory bowel disease. Cell 2008;134:743–56.
[11] Nishikimi T, Maeda N, Matsuoka H. The role of natriuretic peptides in cardioprotection. Cardiovasc Res 2006;69:318–28.
[12] Back SH, Lee K, Vink E, Kaufman RJ. Cytoplasmic IRE1alpha-mediated XBP1 mRNA splicing in the absence of nuclear processing and endoplasmic reticulum stress. J Biol Chem 2006;281:18691–706.
[13] Fu HY, Minamino T, Tsukamoto O, Sawada T, Asai M, Kato H, et al. Overexpression of endoplasmic reticulum-resident chaperone attenuates cardiomyocyte death induced by proteasome inhibition. Cardiovasc Res 2008;79:600–10.
[14] Dignam JD, Lebovitz RM, Roeder RG. Accurate transcription initiation by RNA polymerase II in a soluble extract from isolated mammalian nuclei. Nucleic Acids Res 1983;11:1475–89.
[15] Horio T, Nishikimi T, Yoshihara F, Matsuo H, Takishita S, Kangawa K. Inhibitory regulation of hypertrophy by endogenous atrial natriuretic peptide in cultured cardiac myocytes. Hypertension 2000;35:19–24.
[16] Dally S, Monceau V, Corvazier E, Bredoux R, Raies A, Bobe R, et al. Compartmentalized expression of three novel sarco/endoplasmic reticulum Ca2+ATPase 3 isoforms including the switch to ER stress, SERCA3f, in non-failing and failing human heart. Cell Calcium 2009;45:144–54.
[17] Woodard GE, Rosado JA. Recent advances in natriuretic peptide research. J Cell Mol Med 2007;11:1263–71.
[18] Akazawa H, Komuro I. Roles of cardiac transcription factors in cardiac hypertrophy. Circ Res 2003 May 30;92(10):1079–88.
[19] Newell CL, Deisseroth AB, Lopez-Berestein G. Interaction of nuclear proteins with an AP-1/CRE-like promoter sequence in the human TNF-alpha gene. J Leukoc Biol 1994;56:27–35.
[20] Barabitskaja O, Foulke Jr JS, Pati S, Bodor J, Reitz Jr MS. Suppression of MIP-1beta transcription in human T cells is regulated by inducible cAMP early repressor (ICER). J Leukoc Biol 2006;79:378–87.
[21] LaPointe MC. Molecular regulation of the brain natriuretic peptide gene. Peptides 2005;26:944–56.

Fig. 4. Spliced XBP1 binds to an AP1/CRE-like element in the BNP promoter region and increases its promoter activity. (A) Mapping of the XBP1-response element in the BNP promoter. Luciferase activity from 3 independent experiments was normalized to Renilla luciferase activity before being compared with the control (pGL3) with and without co-transfection of spliced XBP1. Relative luciferase activity was determined as the average of duplicate measurements in 3 independent experiments. *$P<0.05$ versus control (pGL3). (B) Comparative analysis of the sequence of the AP1/CRE-like element in the BNP promoter. (C, D) Effects of deletion of the AP-1/CRE-like region on BNP promoter activity stimulated by spliced XBP1 or NE (1 μmol/L). The pGL3-BNP-luciferase reporter (−1780/+63) with or without the AP-1/CRE-like element was transfected as described in (A). Experiments were repeated twice independently ($n=2$ per experiment). Relative luciferase activity was determined by averaging duplicate measurements in the 3 independent experiments. *$P<0.05$ versus control (pGL3). (E) Binding of spliced XBP1 to the AP1/CRE-like element in the BNP promoter was demonstrated by the ChIP assay. Chromatin was immunoprecipitated with IgG or an antibody for XBP1. Purified precipitates were analyzed by PCR using primers specific for the AP1/CRE-like element (P3/P4) or the region 3 kb upstream of the BNP promoter (P1/P2).

[22] Yoshida H, Haze K, Yanagi H, Yura T, Mori K. Identification of the cis-acting endoplasmic reticulum stress response element responsible for transcriptional induction of mammalian glucose-regulated proteins. Involvement of basic leucine zipper transcription factors. J Biol Chem 1998 Dec 11;273(50):33741–9.
[23] Mao W, Iwai C, Qin F, Liang CS. Norepinephrine induces endoplasmic reticulum stress and downregulation of norepinephrine transporter density in PC12 cells via oxidative stress. Am J Physiol Heart Circ Physiol 2005;288:H2381–9.
[24] Mao W, Iwai C, Keng P, Vulapalli R, Liang CS. Norepinephrine-induced oxidative stress causes PC-12 cell apoptosis by both endoplasmic reticulum stress and mitochondrial intrinsic pathway: inhibition of phosphatidylinositol 3-kinase survival pathway. Am J Physiol Cell Physiol 2006;290:C1373–84.
[25] Colucci WS, Elkayam U, Horton DP, Abraham WT, Bourge RC, Johnson AD, et al. Intravenous nesiritide, a natriuretic peptide, in the treatment of decompensated congestive heart failure. Nesiritide Study Group. N Engl J Med 2000;343:246–53.

nature
cell biology

AMPK controls the speed of microtubule polymerization and directional cell migration through CLIP-170 phosphorylation

Atsushi Nakano[1,4], Hisakazu Kato[3,4], Takashi Watanabe[5,6], Kyung-Duk Min[1,3], Satoru Yamazaki[1], Yoshihiro Asano[3,4], Osamu Seguchi[1], Shuichiro Higo[3], Yasunori Shintani[3], Hiroshi Asanuma[1], Masanori Asakura[1], Tetsuo Minamino[3], Kozo Kaibuchi[6], Naoki Mochizuki[2], Masafumi Kitakaze[1] and Seiji Takashima[3,4,7]

AMP-activated protein kinase (AMPK) is an energy-sensing Ser/Thr protein kinase originally shown to be regulated by AMP[1]. AMPK is activated by various cellular stresses that inhibit ATP production or stimulate ATP consumption[2]. In addition to its role in metabolism, AMPK has recently been reported to reshape cells by regulating cell polarity and division[3–6]. However, the downstream targets of AMPK that participate in these functions have not been fully identified. Here, we show that phosphorylation of the microtubule plus end protein CLIP-170 by AMPK is required for microtubule dynamics and the regulation of directional cell migration. Both inhibition of AMPK and expression of a non-phosphorylatable CLIP-170 mutant resulted in prolonged and enhanced accumulation of CLIP-170 at microtubule tips, and slower tubulin polymerization. Furthermore, inhibition of AMPK impaired microtubule stabilization and perturbed directional cell migration. All of these phenotypes were rescued by expression of a phosphomimetic CLIP-170 mutant. Our results demonstrate, therefore, that AMPK controls basic cellular functions by regulating microtubule dynamics through CLIP-170 phosphorylation.

Besides the metabolic activity of AMPK, there is growing evidence that AMPK and its upstream kinase liver kinase B1 (LKB1) have pivotal roles in the establishment of cell polarity and cell division[7,8] in *Drosophila melanogaster*[6,9] and *Caenorhabditis elegans*[10]. In mammalian cells, AMPK is associated with tight junction assembly, and regulates epithelial polarity[3,4].

To discover previously unidentified substrates of AMPK, we performed a unique screen using two-step column chromatography combined with an *in vitro* kinase reaction. Using mouse heart homogenates, we purified and identified a cytoplasmic linker protein CLIP-170, which has a relative molecular mass of 170,000 (M_r 170K) and is a substrate of AMPK (Supplementary Information, Fig. S1). CLIP-170 is one of the microtubule plus end proteins originally identified as proteins that bind endocytic vesicles to microtubules[11,12]. CLIP-170 directly binds freshly polymerized distal ends of growing microtubules and rapidly dissociates from the older microtubule lattice[13]. However, a direct link between CLIP-170 and physiological control of cell function has not been fully elucidated. Both recombinant AMPK made by 293T cells and AMPK purified from rat liver efficiently phosphorylated recombinant CLIP-170 (Fig. 1a). Phospho amino acid analysis revealed that AMPK phosphorylates a Ser residue of CLIP-170 (Fig. 1b). A combination of mass spectrometric and multiple mutation analyses of CLIP-170 identified Ser 311 as the only AMPK phosphorylation site. AMPK did not phosphorylate CLIP-115, a close mammalian homologue of CLIP-170, or Ser 737 of CLIP-170, demonstrating an AMPK substrate consensus sequence[14] (Fig. 1c). Recombinant glutathione S-transferase (GST)-fused wild-type CLIP-170 and a Ser 311-to-Ala mutant (S311A) of CLIP-170 were produced in *Escherichia coli*. The wild-type, but not the S311A mutant, was phosphorylated by AMPK and 0.29 mole of phosphate per mole of CLIP-170 was incorporated, indicating that Ser 311 of CLIP-170 is phosphorylated directly by AMPK (Fig. 1d). Next, we generated an antibody against Ser 311-phosphorylated CLIP-170 (p-CLIP-170). The specificity and sensitivity of this antibody were confirmed by the following observations: first the p-CLIP-170 antibody exclusively detected p170 as a single band, even when total cell lysates were assessed; and second, it did not recognize phosphatase-treated p170 (Fig. 1e). Analyses using this antibody also demonstrated the specific phosphorylation of CLIP-170 at Ser 311 by AMPK (Fig. 1f). The amino acid sequence surrounding Ser 311 matches the consensus sequence of a potential AMPK phosphorylation site and is well conserved among various species (Fig. 1g).

[1]Division of Cardiovascular Medicine, National Cardiovascular Center and [2]Department of Structural Analysis, National Cardiovascular Center, Research Institute Suita, Osaka 565-8565, Japan. [3]Department of Cardiovascular Medicine and [4]Department of Molecular Cardiology, Osaka University Graduate School of Medicine Suita, Osaka 565-0871, Japan. [5]Institute for Advanced Research, Nagoya University Graduate School of Medicine and [6]Department of Cell Pharmacology, Nagoya University Graduate School of Medicine, Nagoya, Aichi 466-8550, Japan.
[7]Correspondence should be addressed to S.T. (e-mail: takasima@medone.med.osaka-u.ac.jp)

Received 4 March 2010; accepted 29 April 2010; published online 23 May 2010; DOI: 10.1038/ncb2060

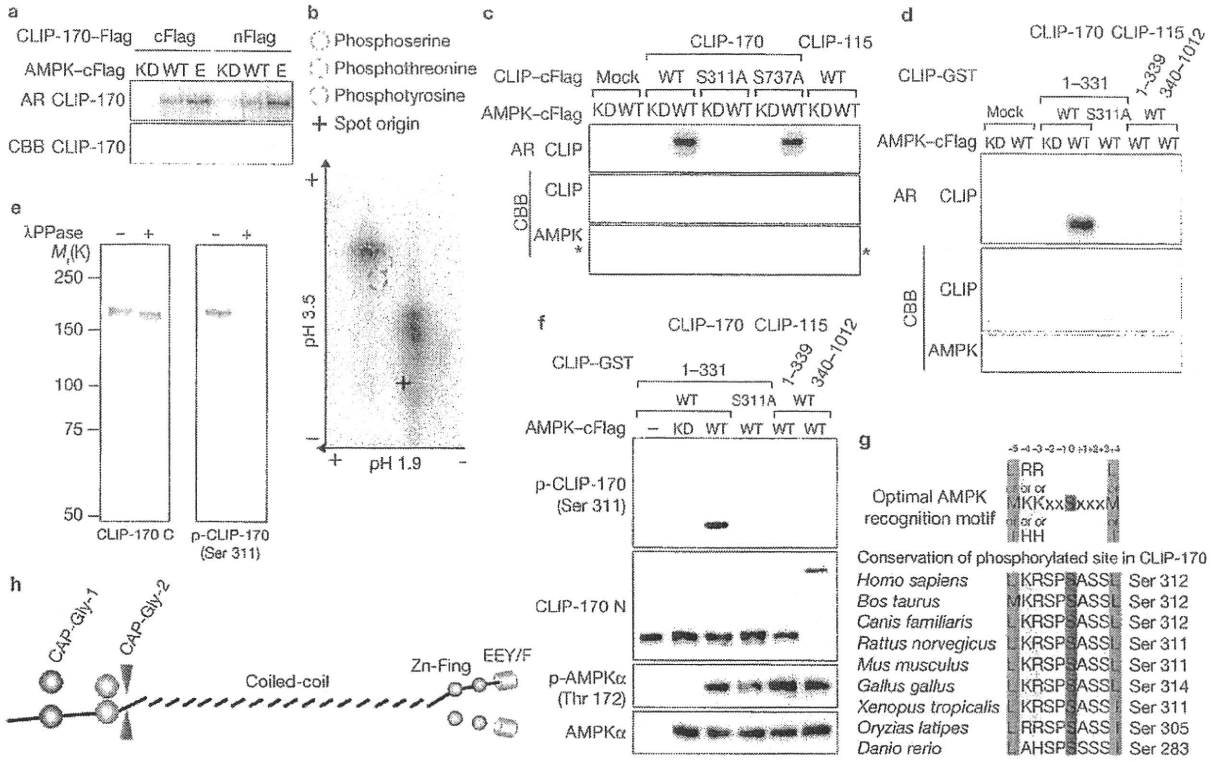

Figure 1 *In vitro* phosphorylation of CLIP-170 Ser311 by AMPK. (a) An autoradiographic (AR) image of mammalian recombinant carboxy-terminally (cFlag) or amino-terminally (nFlag) Flag-tagged CLIP-170 incubated with either recombinant kinase dead (KD), wild-type (WT) or endogenous (E) AMPK. (b) Phospho-amino acid analysis of CLIP-170 phosphorylated by AMPK. Only a Ser residue was phosphorylated (radioactivity indicated by the red circle). (c) An AR of mammalian recombinant cFlag-tagged CLIP-170 (WT, S311A and S737A) and CLIP-115 (WT) incubated with recombinant KD or WT AMPK. AMPK is indicated by an asterisk. (d) An AR image of GST fusion proteins representing amino acids 1–331 of CLIP-170 (WT or S311A), or either the N (1–339) or the C (340–1012) terminus of CLIP-115 incubated with KD or WT AMPK. (e) Lysate of Vero cells treated with or without phosphatase (λPPase) was subjected to immunoblot analysis with an antibody against the C terminus of CLIP-170 (CLIP-170 C) and a Ser 311 phosphospecific antibody (p-CLIP-170). (f) Immunoblot analysis of the GST-fused CLIP constructs described above with KD or WT AMPK. These samples were blotted using a p-CLIP-170 and a non-phosphospecific antibody against the N terminus of CLIP-170 (CLIP-170 N). CLIP-170 N also recognized CLIP-115. (g) The optimal AMPK recognition motif. The consensus sequence of AMPK is identical to the sequence around Ser 311 of CLIP-170. This residue is highly conserved among various species. (h) Structural model of CLIP-170. Ser 311 is located between the CAP-Gly-2 domain and the coiled-coil region in CLIP-170. Ser 311 is indicated by red arrowheads. CAP-Gly, cytoskeleton-associated protein Gly-rich; Zn-Fing, C-terminal zinc knuckle of CLIP-170; EEY/F, C-terminal amino sequence of CLIP-170; CBB, Coomassie brilliant blue staining. Uncropped images of blots are shown in Supplementary Information, Fig. S5.

Ser 311 is located between a Gly-rich microtubule-binding domain (cytoskeleton-associated protein Gly-rich; CAP-Gly) and a coiled-coil domain (Fig. 1h).

Next, we examined AMPK-induced CLIP-170 phosphorylation in cultured cells. Compound C, an inhibitor of AMPK, reduced the phosphorylation level of CLIP-170 (Fig. 2a), whereas the AMPK activator AICAR (5-aminoimidazole-4-carboxyamide ribonucleoside) did not affect CLIP-170 phosphorylation (Supplementary Information, Fig. S2a). The phosphorylation level of acetyl-CoA carboxylase (ACC), which was used as a control, reflected the conventional responses of cells to both Compound C and AICAR. Although Compound C is an inhibitor of AMPK, it can also inhibit several other kinases[15]. Therefore, we used short interfering RNAs (siRNAs) to specifically deplete AMPK. Depletion of AMPK with siRNAs specific for either the α_1 or the α_2 catalytic subunit also reduced CLIP-170 phosphorylation (Fig. 2b). These data indicate that phosphorylation of CLIP-170 at Ser 311 is regulated endogenously by AMPK. To explore the significance of AMPK-induced CLIP-170 phosphorylation, we first immunocytochemically investigated the localization of phosphorylated CLIP-170 in cultured cells. A non-phospho-specific antibody (CLIP-170 C), as well as a Ser 311 phospho-specific antibody (p-CLIP-170), stained the plus ends of microtubules (Fig. 2c, d). To distinguish between the total CLIP-170 population and phosphorylated CLIP-170, Vero cells stably expressing CLIP-170–EGFP were stained with these antibodies. The pattern observed with the CLIP-170 C antibody (red or yellow) completely matched that of CLIP-170–EGFP (Fig. 2e, green), suggesting that CLIP-170–EGFP mimics the localization of endogenous CLIP-170. By contrast, p-CLIP-170 staining mostly overlapped with CLIP-170–EGFP but was located predominantly on the distal side (red or yellow) of CLIP-170–EGFP (Fig. 2f, green). This result suggests that phosphorylated CLIP-170 attaches to microtubules at the more distal end, compared with non-phosphorylated CLIP-170. A marked change in CLIP-170 localization was observed when these cells were treated with Compound C: CLIP-170–EGFP accumulated significantly farther along the length of the microtubules (Fig. 2g, h, green). CLIP-170 C staining again overlapped with CLIP-170–EGFP (Fig. 2g, red or yellow), whereas p-CLIP-170 staining was markedly reduced and localized as only a tiny

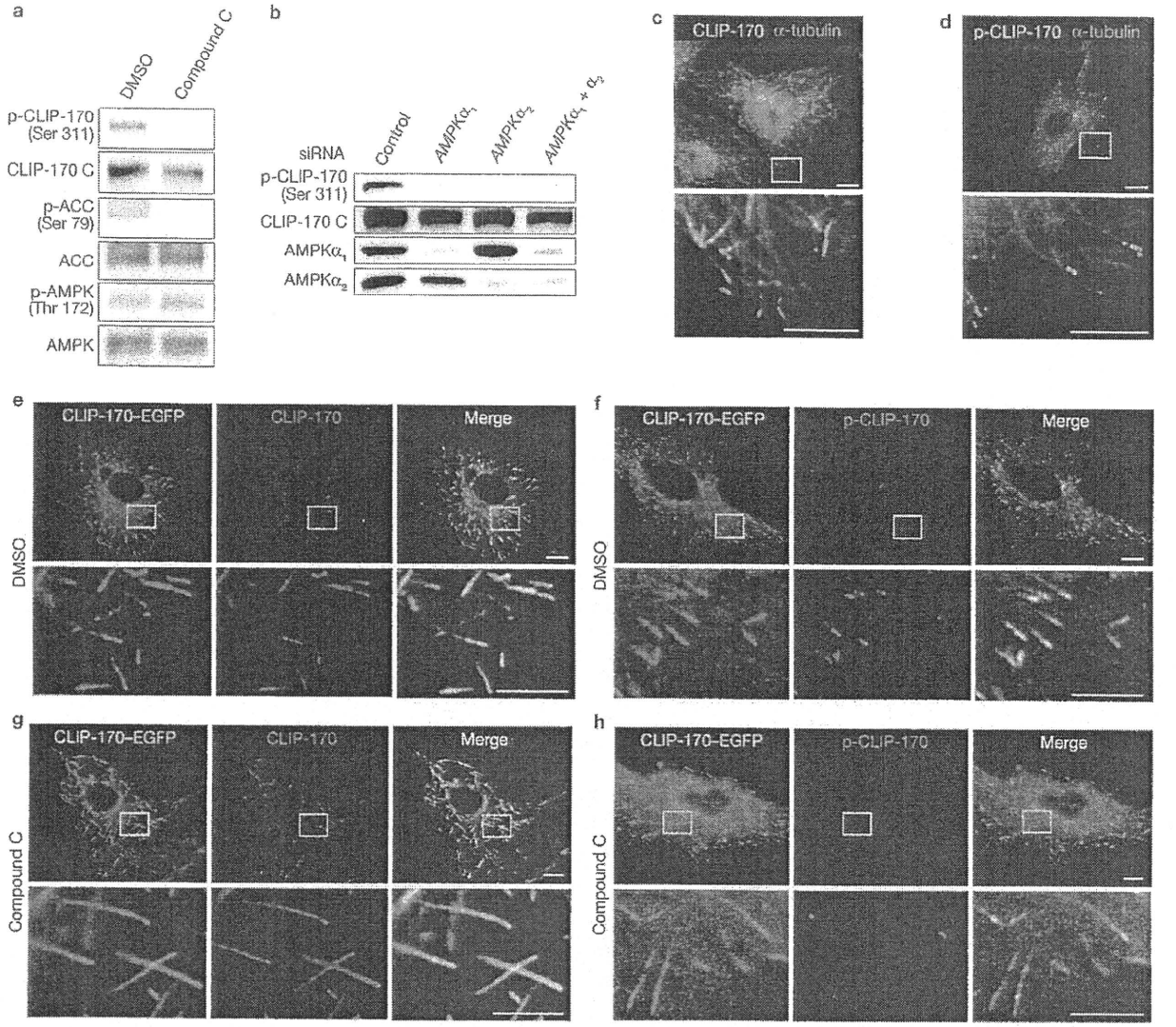

Figure 2 CLIP-170 phosphorylated by AMPK localizes to microtubule tips. (**a**) Immunoblot analysis of the phosphorylation level of CLIP-170, AMPK, and ACC in cells treated with 0.2% DMSO or Compound C (20 μM). CLIP-170 C is a non-phosphospecific antibody that recognizes the C terminus of CLIP-170. (**b**) Immunoblot analysis of the phosphorylation level of CLIP-170 and the expression level of AMPKα_1 and α_2 in cells treated with siRNA targeting *AMPK*α_1, α_2, or both subunits of AMPK. (**c**) Immunostained images of Vero cells stained with anti-α-tubulin and the anti-CLIP-170 C antibodies. (**d**) Immunostained images of Vero cells stained with α-tubulin and p-CLIP-170 antibodies. (**e**, **f**) Immunostained images of Vero cells stably expressing CLIP-170–EGFP (GFP image, left) and treated with DMSO as a control. These cells were stained with a CLIP-170 C antibody (**e**, centre) or a p-CLIP-170 antibody (**f**, centre). (**g**, **h**) Immunostained images of Vero cells stably expressing CLIP-170–EGFP (GFP image, left) and treated with Compound C. These cells were stained with a CLIP-170 C antibody (**g**, centre) or a p-CLIP-170 antibody (**h**, centre). The merged images of each panel are shown on the right. The white boxed regions in the panels are enlarged below each panel. Scale bars, 10 μm (**c**–**h**, upper rows) and 5 μm (**c**–**h**, bottom rows). Uncropped images of blots are shown in Supplementary Information, Fig. S5.

spot within the CLIP-170–EGFP-positive region (Fig. 2h, red or yellow). Most of the CLIP-170 on microtubules, therefore, was non-phosphorylated, and a small amount of phosphorylated CLIP-170 accumulated at the distal ends. To examine the precise distribution of CLIP-170 on the microtubules under AMPK-inhibited conditions, linescan analysis along the microtubules was performed using double immunocytochemistry with CLIP-170 C and tubulin antibodies. We separately measured total CLIP-170 associated with microtubule plus ends, and CLIP-170 associated with the outermost microtubule tips (within a 0.129-μm square box at the very end of the microtubules). When compared with the DMSO control Compound C treatment increased the association of CLIP-170 with microtubules both in the whole tip (6-fold) and at the outer tip (1.7-fold) (Supplementary Information, Fig. S2b–d). Depletion of both AMPKα_1 and α_2 by siRNA also resulted in accumulation of CLIP-170 on microtubule plus ends, similarly to inhibition by Compound C (Supplementary Information, Fig. S2e, f). This characteristic change of CLIP-170 localization prompted us to examine the role of AMPK in the regulation of microtubule dynamics.

To study how AMPK regulates microtubule dynamics, we examined the behaviour of CLIP-170 in living cells. First, we tested whether phosphorylation levels of CLIP-170 affected polymerization of microtubules.

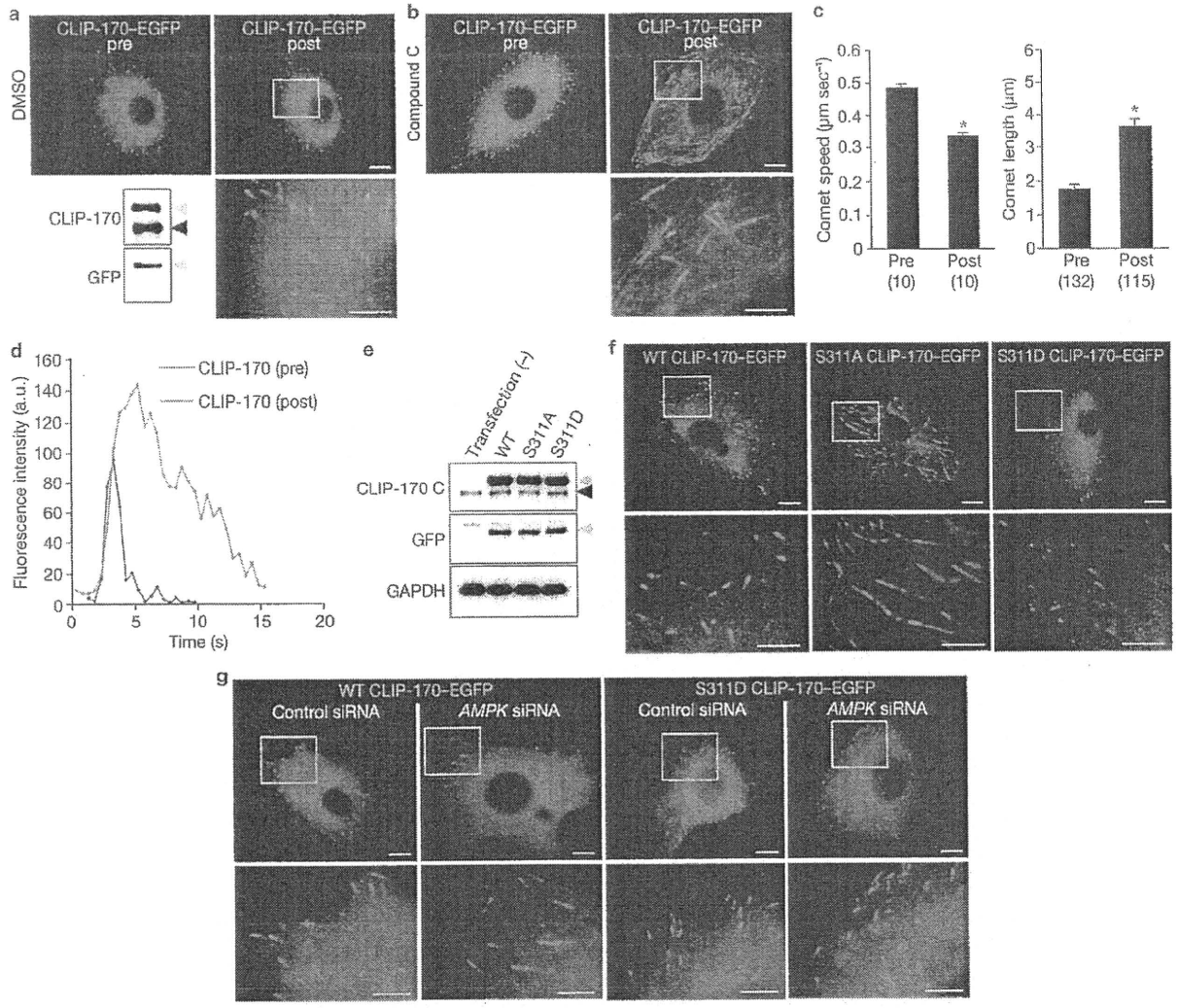

Figure 3 AMPK-phosphorylated CLIP-170 regulates microtubule dynamics. (**a**, **b**) GFP images of Vero cells stably expressing CLIP-170–EGFP before (pre) and 10 min after (post) treatment with 0.2% DMSO control (**a**) or Compound C (20 μM, **b**). The immunoblot on the left shows exogenous CLIP-170–EGFP (grey arrowheads) and endogenous CLIP-170 (black arrowhead). (**c**) Bar graphs showing the speed (left panel) and length (right panel) of a single comet before (pre) and 10 min after (post) Compound C treatment in the same cell. Values are means ± s.e.m.; *n* shown in parentheses; $^{*}P < 0.01$, compared with pre. (**d**) Fluorescence intensity plots of CLIP-170–EGFP of the same cell before (pre, blue) and 10 min after (post, red) Compound C treatment. (**e**) Expression levels of wild-type (WT), S311A and S311D CLIP-170–EGFP in transiently transfected Vero cells were comparable, as determined by immunoblotting using the antibodies indicated on the left. The grey and black arrowheads indicate GFP-tagged exogenous CLIP-170 and endogenous CLIP-170, respectively. (**f**) GFP images of cells transiently expressing WT (left), S311A (centre) and S311D (right) CLIP-170–EGFP. (**g**) GFP images of the cells transiently expressing WT and S311D CLIP-170–EGFP treated with control siRNA or siRNA targeting both *AMPK*α_1 and α_2. White boxed regions in the panels are enlarged below each panel. Scale bars, 10 μm (**a**, **b**, **f**, **g**, upper panels) and 5 μm (**a**, **b**, **f**, **g**, enlarged images). Uncropped images of blots are shown in Supplementary Information, Fig. S5.

By live-cell imaging, we observed that stably expressed CLIP-170–EGFP accumulated at the distal ends of microtubules and seemed to move like a comet from the centrosome to the cell periphery (as shown in sequential images converted to video, Supplementary Information, Movie 1). The speed of the CLIP-170 comets coincided with that of microtubule polymerization[16,17]. Consistent with our results in fixed cells (Fig. 2), 10-min inhibition of AMPK by Compound C in living cells also resulted in elongated CLIP-170 comets, compared with control DMSO-treated cells (Fig. 3a–c). Moreover, the speed of the comets was reduced by Compound C (Fig. 3c; Supplementary Information, Movie 2). To analyse the CLIP-170 behaviour more precisely, we measured the fluorescence intensity values along the CLIP-170–EGFP tracks over time in the same living cells before and 10 min after Compound C treatment. This fluorescence intensity analysis of CLIP-170–EGFP demonstrated that Compound C markedly increased the peak fluorescence intensity and slowed the dissociation of CLIP-170 from the older part of the microtubules (Fig. 3d). Using the same cell line stably expressing CLIP-170–EGFP, depletion of AMPK by siRNA also reduced the speed of the comets and increased the length of CLIP-170 comets (Supplementary Information, Fig. S2g–i, Movie 3). To elucidate the specific role of CLIP-170 Ser 311 phosphorylation by AMPK, we compared the phenotypes of cells transiently transfected with wild-type and two Ser 311 mutants of CLIP-170. S311A CLIP-170–EGFP

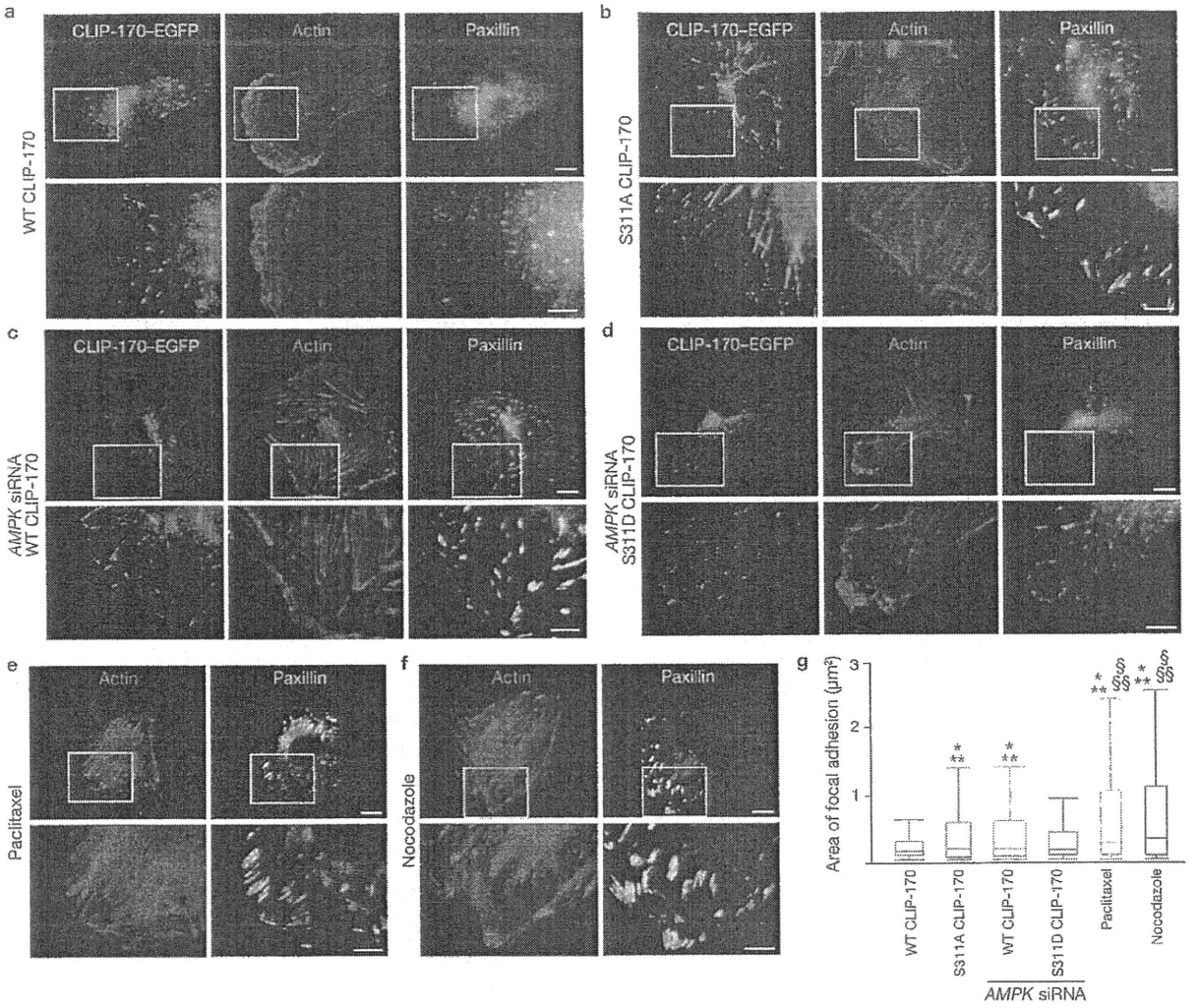

Figure 4 Loss of CLIP-170 phosphorylation increases the size of focal adhesions. (a, b) Immunostained images of Vero cells transiently expressing wild-type (WT; a) and S311A (b) CLIP-170–EGFP (GFP image, left). These cells were stained with fluorescein-conjugated phalloidin (centre) and a paxillin antibody (right) to visualize actin microfilaments and focal adhesions, respectively. (c, d) Immunostained images of Vero cells transiently expressing WT (c) and S311D (d) CLIP-170–EGFP (GFP image, left) treated with siRNA targeting both *AMPK*α_1 and α_2. These cells were stained with fluorescein-conjugated phalloidin (centre) and a paxillin antibody (right). (e, f) Immunostained images of Vero cells treated with 5 μM paclitaxel (e) or 10 μM nocodazole (f). These cells were stained with fluorescein-conjugated phalloidin (left) and a paxillin antibody (right). The white boxed regions in the panels are enlarged below each panel. Scale bars, 10 μm (a–f, upper row) and 5 μm (a–f, bottom row). (g) Box and whisker plots of the area stained with a paxillin antibody showing the 25th percentile (bottom line of each box), median (middle line of each box), 75th percentile (top line of each box), and the 5th and 95th percentiles (each whisker); $n = 10$ for each group; $^{*}P < 0.01$, compared with WT CLIP-170; $^{**}P < 0.01$, compared with S311D CLIP-170 treated with *AMPK* siRNA; $^{\S}P < 0.01$, compared with S311A CLIP-170; $^{\S\S}P < 0.01$, compared with WT CLIP-170 treated with *AMPK* siRNA.

is a non-phosphorylatable mutant, and a Ser 311-to-Asp mutant (S311D CLIP-170–EGFP) is a phosphomimetic mutant. These EGFP fusion proteins were equally expressed in Vero cells (Fig. 3e). S311A CLIP-170–EGFP accumulated as comets with longer tails and moved more slowly than wild-type CLIP-170–EGFP (Fig. 3f centre; Supplementary Information, Table S1, Movie 4). By contrast, S311D CLIP-170–EGFP had the same comet length and moved with the same speed as wild-type CLIP-170–EGFP (Fig. 3f, right; Supplementary Information, Table S1, Movie 5). These findings are consistent with the observation that most of the endogenous CLIP-170 was phosphorylated by AMPK. Furthermore, S311D CLIP-170–EGFP rescued the phenotypes caused by siRNA depletion of AMPK (Fig. 3g; Supplementary Information, Table S1, Movie 6). Also, in the cells treated with Compound C, transfection of S311D CLIP-170–EGFP restored comet speed and length. Quantitative data of comet speed and length in various conditions are summarized in Supplementary Information, Table S1.

CLIP-170 binds only to the growing phase of microtubules. To further examine microtubule dynamics during the shortening phase, Vero cells stably expressing α-tubulin–EGFP were observed before and 10 min after Compound C treatment. Compound C markedly decreased the microtubule shortening distance (Supplementary Information, Fig. S2j, Movie 7). This change in microtubule behaviour may stabilize microtubules. We then observed microtubule stability by staining them with an antibody against detyrosinated tubulin (Glu tubulin,

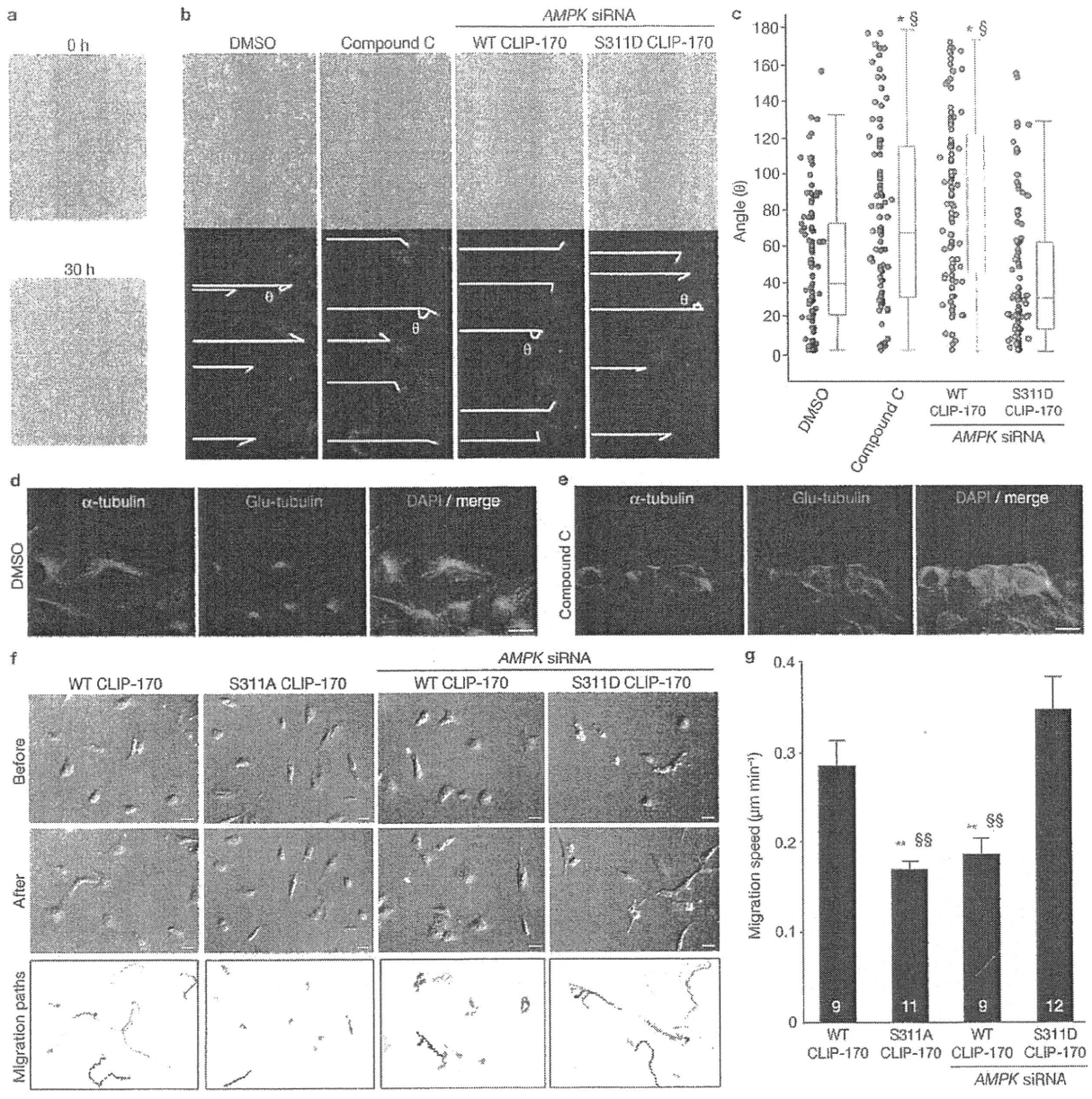

Figure 5 Phosphorylation of CLIP-170 at Ser 311 is essential for cell polarity and directional cell migration. (**a**) Phase contrast microscopy images of Vero cells before (upper panel) and 30 h after (lower panel) scratch. (**b**) Phase contrast microscopy images (upper panels) and immunostained images of Vero cells stained with a γ-tubulin antibody (lower panels) after being subjected to a scratch assay. Images were captured 12 h after incubation. The cells were treated by either repeated administration of DMSO control or Compound C, or transiently transfected with wild-type (WT) or S311D CLIP-170 and siRNA targeting both *AMPKα*$_1$ and *α*$_2$. To assess cell polarity, the angles (θ) between the lines of γ-tubulin and the scratched line at the centre of each nucleus were measured as a marker for MTOC reorientation (lower panels). (**c**) Box and whisker plots of angles (θ) with actual data points shown on the left; n=100 per group; $^*P$ <0.01, compared with DMSO; $^{\S}P$ <0.01, compared with S311D CLIP-170 treated with *AMPK* siRNA. (**d**, **e**) Images of Vero cells immunostained with an α-tubulin (left, green) and a detyrosinated (Glu) tubulin antibody (centre, red) after being subjected to a scratch assay following repeated treatment with control DMSO (**d**) or Compound C (**e**) for 6 h. DAPI stained nucleus (blue). The merged images of each panel are shown on the right. Scale bars, 20 μm. (**f**) Time lapse images acquired by differential interference contrast of cells transiently expressing WT, S311A, and WT or S311D CLIP-170 treated with siRNA targeting both *AMPKα*$_1$ and *α*$_2$. Images acquired before (upper line of each panel) and after 12 h (middle line of each panel) are shown. The bottom row of each panel shows the individual paths of migrating cells over 12 h. Scale bars, 30 μm. (**g**) Bar graphs showing the migration speed of the cells from (**f**); Numbers in the bars indicate n. Values represent means ± s.e.m; $^{**}P$ <0.01, compared with WT CLIP-170. $^{\S\S}P$ <0.01, compared with S311D CLIP-170 treated with *AMPK* siRNA.

named for the newly exposed C-terminal glutamate residue). The amount of stable microtubules was greater in cells transiently expressing S311A CLIP-170–EGFP (Supplementary Information, Fig. S3b) than in cells transiently expressing wild-type CLIP-170 (Supplementary Information, Fig. S3a). Cell depleted of AMPK by siRNA (Supplementary Information, Fig. S3g), or treated with Compound C (Supplementary

Information, Fig. S3d) also showed the same phenotype as cells expressing S311A CLIP-170. These phenotypes were rescued by S311D CLIP-170 (Supplementary Information, Fig. S3f, i). Collectively, these data suggest that phosphorylation of CLIP-170 at Ser 311 by AMPK is necessary for proper CLIP-170 dissociation from microtubules, and that this modification of CLIP-170 is essential for efficient polymerization and depolymerization of microtubules. Dynamic modulation of microtubule polymerization and stability by AMPK-phosphorylated CLIP-170 might represent a previously unknown mechanism through which AMPK establishes cell polarity. Therefore, we further examined the role of CLIP-170 phosphorylation by AMPK during cell polarization and subsequent cell migration.

During cell migration, microtubules target focal adhesions and regulate cell–extracellular matrix (ECM) adhesion[18–20]. Thus, we first examined whether phosphorylation of CLIP-170 at Ser 311 affects the size of focal adhesions. Isolated Vero cells transiently expressing wild-type CLIP-170–EGFP formed an actin meshwork in protruding lamellipodium. Furthermore, staining focal adhesions with a paxillin antibody revealed small, scattered spots located predominantly at the protruding lamellipodium (Fig. 4a). By contrast, expression of S311A CLIP-170–EGFP caused loss of lamellipodium formation and adhesion maturation, which resulted in significantly enlarged spots (Fig. 4b). Similar phenotypes were observed when AMPK was depleted by siRNA (Fig. 4c) or inhibited by Compound C (Supplementary Information, Fig. S4b). These AMPK depletion phenotypes were almost completely rescued by the expression of S311D CLIP-170–EGFP (Fig. 4d, g; Supplementary Information, Fig. S4d). Treatment with paclitaxel and nocodazole (Fig. 4e, f), both of which disturb microtubule dynamics, resulted in similar phenotypes of abnormal size of focal adhesion as cells expressing S311A CLIP-170–EGFP and cells depleted of AMPK. These data indicate that AMPK-dependent phosphorylation of CLIP-170 regulates the size of focal adhesions by regulating microtubule dynamics. The fact that inhibiting AMPK-induced phosphorylation of CLIP-170 altered the size of focal adhesions and lamellipodium formation suggests an important role of the AMPK–CLIP-170 signalling axis in cell polarity and migration. We examined the effect of AMPK inhibition on cell polarity using the scratch assay. The leading cells started to polarize and migrated towards a scratched line, closing the gap in about 30 h (Fig. 5a). However, repeated treatment with Compound C and depletion of AMPK by siRNA both inhibited closure of the gap and interfered with microtubule-organizing centre (MTOC) reorientation in leading cells. Expression of S311D CLIP-170 rescued AMPK depletion (Fig. 5b, c; Supplementary Information, Fig S4g, h). The first two layers of the leading cells showed that the stabilized microtubules stained with a detyrosinated (anti-Glu) tubulin antibody were clearly polarized towards the leading edge (Fig. 5d). By contrast, AMPK inhibition by Compound C increased the amount of stable microtubules, which lost their orientation towards the leading edge (Fig. 5e). Finally, we tested the effect of CLIP-170 phosphorylation on free cell migration. Wild-type CLIP-170-expressing cells migrated with active lamellipodium formation. By contrast, S311A CLIP-170-expressing cells and wild-type CLIP-170-expressing cells treated with *AMPK* siRNA showed diminished migration and fewer membrane extensions (Fig. 5f). Again, expression of S311D CLIP-170 rescued the effect of siRNA *AMPK* knockdown of (Fig. 5g; Supplementary Information, Movie 8). These data suggest that AMPK-induced phosphorylation of CLIP-170 is required to establish front–rear polarity and proper cell migration, presumably through the regulation of microtubule tip dynamics.

We have shown here that CLIP-170 is a strong candidate AMPK substrate that regulates cell polarity through alteration of its dynamics on the plus ends of microtubules. Recently, abnormal mitotic phenotypes were observed for both *AMPK*- and *LKB1*-null *Drosophila*. They demonstrated that AMPK phosphorylates myosin regulatory light chain (MRLC) directly, and a phosphomimetic MRLC transgene rescued the polarity phenotypes induced by loss of the AMPK pathway[6]. However, the transgene did not rescue all phenotypes, suggesting that AMPK signalling is mediated by additional downstream targets.

The dynamics of CLIP-170 on microtubules were recently and precisely investigated both *in vitro* and *in vivo*[13,17]. In these reports, CLIP-170 turnover on microtubules was rapid, and the diffusion of CLIP-170 was rate-limiting for its binding to microtubule plus ends. They also showed that the ends of growing microtubules contain a surplus of sites to which CLIP-170 can bind, and the older lattice has a lower affinity for CLIP-170 than the newer, growing ends of the microtubules. These changes in the affinity of plus end proteins for microtubules may be essential for their effects on microtubule dynamics.

We could not demonstrate an altered affinity of phosphorylated CLIP-170 for the microtubule plus end *in vitro* because of the difficulty associated with reconstituting the plus end as *in vivo*. However, we speculate, for the following reasons, that non-phosphorylated CLIP-170 increased its affinity to microtubules. First, linescan analysis showed that depletion of AMPK activity increased the association not only of total CLIP-170 with the microtubule but also of CLIP-170 at the outer tip. Second, the fluorescence intensity analysis measured in living cells indicated that non-phosphorylated CLIP-170 increased the peak fluorescence intensity and slowed its dissociation from the plus end of microtubules. Third, phosphorylated CLIP-170 localized within the more distal portion of the total CLIP-170 population. These results support the hypothesis that the phosphorylation status of CLIP-170 at Ser 311 determines its affinity for microtubules. Because CLIP-170 turnover on microtubules is rapid, phosphorylation may be a suitable modification to regulate its affinity for microtubules. We conclude that phosphorylation of CLIP-170 alters its affinity for microtubule plus ends and that this phenomenon might contribute to the rapid turnover of CLIP-170, which is necessary for efficient microtubule polymerization.

The observation that the phosphorylation status of CLIP-170 regulates the growth rate of microtubules has not been reported. The precise mechanisms remain unclear; however we speculate that Ser 311 phosphorylation is necessary to reduce the affinity of CLIP-170 for the microtubule lattice and promote the efficient turnover of CLIP-170 at the plus end, similarly to a microtubule polymerase.

Another intriguing phenotype of AMPK depletion is the marked enhancement of microtubule stabilization in migrating cells. Moreover, AMPK depletion impaired the polarized stabilization of microtubules towards the leading edge. AMPK depletion not only reduced the speed of polymerization but also decreased the shortening distance of microtubules. Because both phenomena prolong the lifetime of microtubules, these two changes might cause the ubiquitous enhancement of microtubule stabilization.

Expression of the non-phosphorylatable CLIP-170 S311A mutant and depletion of AMPK disrupted front–rear polarity and reduced cell migration. The precise mechanisms of this phenotype are unclear, but decreased